
International Journal of
Young Scientist
Research
Vol 9, No. 1, June 2025
ISSN: 2588- 5111
Generated in
https://deepai.org/

Contents

Young Scientist Research

Title proper: Young Scientist Research

Subject: NATURAL SCIENCES, ART, ENGINEERING AND TECHNOLOGY

Corporate contributor: Ariaian Young Innovative Minds Institute

Publisher: Tehran: Ariaian Young Innovative Minds Institute

Dates of publication: 2017- Present

Frequency: Annual

Type of resource: Periodical

Language: English

Country: Iran

Medium: Online

Indexed by: ROAD (The Directory of Open Access Resources)

ISSN- 2588-5111
ISSN International Centre
45 rue de Turbigo
75003 Paris
France

Address:

Unit 14, No.32, Malek Ave., Shariati St.

Post Code: 1565843537

Tel:+9821-77507013, 77522395

WELCOME TO THE INTERNATIONAL JOURNAL of YOUNG SCIENTIST RESEARCH

Young Scientist Research is a research journal based on scientific projects and we are pleased to present our students' work in scientific activities. This open-access journal includes young students' research in any field of science which publishes full-length and abstract research on any aspects of applied sciences in relation to work presented in both national and international conferences, competitions and tournaments of all types.

Programs that have educational opportunities for high school students to present their distinguished projects from regional, national and international events such as International Conference of Young Scientists (ICYS), International / Persian Young Physicists' Tournament (IYPT/ PYPT), International / Iran Physics' Tournament (IPT/ IRPT), International / Persian Young Naturalists' Tournament (IYNT/ PYNT) and International ISAC Olympiad .

New manuscripts sent to the Journal will be handled by the Editorial Office who checks compliance with the guidelines to authors. Then a rapid screening process at which stage a decision to reject or to go to full review is made.

By submission of a manuscript to the Journal, all authors warrant that they have the authority to publish the material and that the paper, or one substantially the same, has neither been published previously, nor is being considered for publication elsewhere.

This journal belongs to Ariaian Young Innovative Minds Institute, AYIMI, and one to two issues are published in a year. All details are on the YOUNG SCIENTIST RESEARCH Journal website (http://journal.ayimi.org).

Editor in Chief
Dr. Dina Izadi
Researcher & President of
Ariaian Young Innovative Minds Institute, AYIMI
ADIB, Cultural and Artistic Institute
http://www.ayimi.org
http://www.ayimi.org/adib
http://journal.ayimi.org
Email: info@ayimi.org
Unit 14, No. 32, Malek Ave., Shariati St.,
Post Code: 1565843537, Tehran/ Iran
Young Scientist Research Journal, ISSN: 2588-5111

CURRENT ISSUE
Vol 9 NO1 June 2025

INDICATOR FEATURE PACKAGING MATERIAL DEVELOPED FROM BACTERIAL CELLULOSE AND AUTONOMOUS USAGE MODEL WITH IMAGE PROCESSING SYSTEM

ZEYNEP DALGIÇ, EFE CANSEVEN, DENIZ ŞEREFHANOĞLU, SEHER DALGIÇ, efecanseven7@gmail.com

ARTICLE INFO

First place in Izmir IISEEF 2024

Accepted by Ariaian Young Innovative Minds Institute , AYIMI

http://www.ayimi.org ,info@ayimi.org

ABSTRACT

Polystyrene containers, which are widely used for packaging raw meat today, pose significant problems in terms of both biodegradability and cost. Additionally, the carcinogenic substances present in polystyrene plastics pose a serious risk to human health due to their direct contact with food. This study focuses on the development of a bacterial cellulose-based indicator packaging material as an alternative to polystyrene, along with an"Early Spoilage Detection System." This packaging material is sustainable, biodegradable, capable of extending the shelf life of food, and cost-effective. This study aims to promote sustainable resource consumption, minimize plastic use and contribute to a cleaner world.

Keywords : *Plastic, Packaging, Sustainability, Bacterial cellulose, Detection system*

1. Introduction

The long-standing and escalating issue of plastic pollution has become a chronic problem for humanity and the planet. The degradation of these plastics in nature takes centuries, and according to the WHO, their carcinogenic content poses a serious risk to human health. It is estimated that only about 9% of the plastic produced to date has been recycled. Moreover, these recycling processes come with significant costs and energy consumption. Given these challenges, the search for alternatives has become imperative. In this context, a study has been developed focusing on the use of sustainable materials, specifically bacterial cellulose (BC). Bacterial cellulose is a biocompatible (Sulaeva et al., 2015), low-cost, durable, and environmentally friendly material (Navya et al., 2022) with potential for use as a packaging material (Shi et al., 2014). Several studies have explored the selection of bacterial strains and fermentation conditions for BC production:

- The production of BC in different nutrient media has been compared (Bae & Shoda, 2005).
- Glucoacetobacter sacchari has been shown to produce BC efficiently in glucose-based media (Travatti et al., 2011).
- BC's high purity, ability to create various textures such as flavor and color changes, thickening, and gelling make it highly suitable for use as a food additive and packaging material (Shi et al., 2014).
- Other studies have addressed challenges related to reactor design for BC production and the optimization of pH balance in fermentation media. The high cost of carbon sources used by bacteria as nutrients has limited its widespread adoption. However, the use of food waste and by-products could reduce costs. BC has potential applications in food and beverage production, the dye industry, paper manufacturing, packaging, filtration materials, and medical applications (Güzel & Akpınar, 2018).

2. Materials and Methods

2.1. BC Disk Preparation

Homemade grape vinegar (500 mL) was mixed with 20 g of powdered sugar and 5 g of brewer's yeast extract diluted in 200mL distilled water in a glass jar. The jar was covered with a double-layered cloth and incubated at room temperature in the dark (Gündüz et al., 2015). A gelatinous layer formed on the surface after two weeks.

2.2. BC Production

To enable continuous production of the BC disk (synthesized by acetic acid bacteria in vinegar) over a large surface area, a simple reactor was prepared in a wide basin: 3 L of boiled (later-cooled) drinking water was mixed with 180 g of sugar, 7 bags of green tea, and 200 mL of vinegar. The BC disk was then placed into this growth medium. The reactor was covered with double-layered cloth and maintained at room temperature. The BC layer formed after one week and harvested.

2.3. Sterilization and Drying of BC

The BC was sterilized by immersion in boiling water, rinsed in sodium bicarbonate solution to neutralize residual acidity from the vinegar, and washed with distilled water. It was then dried at 50°C in an oven until pliable.

2.4. BC Container Fabrication and Indicator Functionalization with Red Cabbage Extract

Red cabbage extract was obtained using a Soxhlet apparatus. Dried BC was molded into container shapes and dyed with the red cabbage extract.

2.5. pH Color Scale Development

Acidic, neutral, and basic solutions were prepared by diluting HCl and NaOH in 30 mL of distilled water. These solutions were added to 30 mL of red cabbage extract to achieve a final volume of 50 mL. The resulting pH-dependent color gradient was used to create an informational color scale for labeling.

2.6. Shelf-Life Experiments

2.6.1) Meat Packaging:

- Ground beef (15 g ± 1 g) was divided into two samples: one wrapped in BC and the other in plastic cling film.
- The same procedure was repeated for chicken meat.

meat.

· Four samples were prepared:

- Experimental group: BC-wrapped beef and BC-wrapped chicken.
- Control group: Plastic-wrapped beef and chicken.

· All samples were refrigerated at +4°C for 2 days (maximum spoilage period for meat products).

2.6.2) Aerobic Bacterial Count:

Aerobic bacterial counts were determined by incubating food samples on nutrient agar at 30°C for 72 hours and enumerating colony-forming units (CFU).

· A 10 g sample was homogenized with 90 mL of Maximum Recovery Diluent (MRD: 1.0 g peptone, 8.5 g sodium chloride, 1 L distilled water). Serial dilutions (10^{-1}) were prepared, and 1 mL aliquots were plated in duplicate across six agar plates.

· Total samples:

- Experimental Beef: 14 plates
- Experimental Chicken: 14 plates
- Control Beef: 14 plates
- Control Chicken: 14 plates
- 1 negative control (uninoculated agar)

· Agar composition: Enzymatically digested casein (5 kg), yeast extract (2.5 kg), dextrose (1 kg), agar (15 kg), and distilled water (1 L).

2.7. Biodegradability of BC in Soil

To assess biodegradability, 75 g of BC and an equivalent mass of plastic foam were buried in soil. Visual and mass loss observations were recorded every 5 days.

2.8. Autonomous Imaging System Design

A robotic imaging system was developed to automate spoilage detection:

· A linear sliding module with LED lighting was mounted on a 50 cm platform. A 3D-printed camera holder was attached to a threaded rod and iron bar, enabling movement via a Nema 17 stepper motor controlled by an Arduino Uno, A4988 driver, and endstop switches.

· The system was programmed using Python, JavaScript, and C++ to calibrate color thresholds, capture images, and analyze spoilage via a Windows interface.

· All components (camera holder, circuit enclosures) were designed in Tinkercad and 3D-printed.

3. Results

1) Shelf-Life Analysis:

Table 1: Aerobic Bacterial Colony Counts in Beef (CFU/g)

Group	Significant Dilution	Mean Results
Control Beef (-2)	460, 466	4.4×10^4
Experimental Beef (-3)	120, 114	1.2×10^4

Table 2: Aerobic Bacterial Colony Counts in Chicken (CFU/g)

Group	Significant Dilutions	Mean Results
Control Chicken (-2)	376, 358	3.4×10^4
Experimental Chicken (-3)	216, 206	2.1×10^4

2) Biodegradability of BC:

After two weeks, BC degraded into crumbled soil particles, while the plastic foam retained its original mass (75 g) and structure.

4. Discussion

BC-wrapped samples exhibited significantly lower bacterial growth compared to plastic-wrapped controls (Tables 1–2). Fresh meat is inherently non-sterile and highly perishable, with spoilage thresholds (5×10^5 CFU/g, per ISO 4833) reached rapidly in control groups. BC's barrier properties likely inhibited microbial proliferation, extending shelf life.

5.Conclusion

BC demonstrates critical advantages for sustainable food packaging:

· Cost-effective production: Fermentation-based synthesis avoids resource-intensive agricultural processes required for plant-based bioplastics.

· Extended shelf life: Reduces bacterial growth in perishable goods.

· Rapid biodegradation: Decomposes without chemical residues, unlike petroleum-based plastics. This study positions BC as a viable, eco-friendly alternative to conventional packaging for raw meats.

Acknowledgments

We thank IISEEF for the opportunity to present this work internationally, represent our institution, and for awarding us the AYIMI Article Prize.

References

[1] Akoğlu, A. ., Karahan, A. G. ., Çakmakçı, M. L. ., Çakır, İ. . (2010). Bakteriyel Selülozun Özellikleri ve Gıda Sanayisinde Kullanımı. Gıda, 35(2), 127-134.

[2] Bae, S. O., & Shoda, M. (2005). Production of bacterial cellulose by Acetobacter xylinum BPR2001 using molasses medium in a jar fermentor. Applied microbiology and biotechnology, 67(1), 45–51. https://doi.org/10.1007/s00253-004-1723-2

[3] Chawla, Prashant & Bajaj, Ishwar & Survase, Shrikant & Singhal, Rekha. (2009). Microbial Cellulose: Fermentative Production and Applications. Food Technology and Biotechnology. 47. 107-124.

[4] Gündüz, G., Aşık, N., Aydemir, D., Kılıç, A. (2017). Bakteriyel Selüloz Üretimi ve Karakterizasyonu. Düzce Üniversitesi Orman Fakültesi Ormancılık Dergisi, 10(2), 1-10.

[5] Güzel, M., & Akpınar, Ö. (2017). KOMAGATAEİBACTER HANSENİİ GA2016 İLE BAKTERİYEL SELÜLOZ ÜRETİMİ VE KARAKTERİZASYONU. Gıda, 42(5), 620-633.

[6] Güzel, M., & Akpınar, Ö. (2018). Bakteriyel Selülozların Üretimi ve Özellikleri ile Gıda ve Gıda Dışı Uygulamalarda Kullanımı. Akademik Gıda, 16(2), 241 -251. https://doi.org/10.24323/akademik-gida.449633

[7] Güzel, M., & Akpınar, Ö. (2018). Bakteriyel Selülozların Üretimi ve Özellikleri ile Gıda ve Gıda Dışı Uygulamalarda Kullanımı. Akademik Gıda, 16(2), 241 -251. https://doi.org/10.24323/akademik-gida.449633

[8] Köksal, Ö., Aydın Er, B., Ardalı, Y., Sağlam, M. (2019). Biyoplastiklerin Biyodegradasyonu. Sinop Üniversitesi Fen Bilimleri Dergisi, 4(2), 151-167. https://doi.org/10.33484/sinopfbd.499862

[9] Navya, P. V., Gayathri, V., Samanta, D., & Sampath, S. (2022). Bacterial cellulose: A promising biopolymer with interesting properties and applications. International journal of biological macromolecules, 220, 435–461. https://doi.org/10.1016/j.ijbiomac.2022.08.056

[10] Ross, P., Mayer, R., & Benziman, M. (1991). Cellulose biosynthesis and function in bacteria. Microbiological reviews, 55(1), 35–58. https://doi.org/10.1128/mr.55.1.35-58.1991

[11] Shi, Zhijun & Zhang, Yue & Phillips, Glyn & Yang, Guang. (2013). Utilization of bacterial cellulose in food. Food Hydrocolloids. 35. 539-545. 10.1016/j.foodhyd.2013.07.012.

[12] Shoda, Makoto & Sugano, Yasushi. (2005). Sugano, Y.: Recent advances in bacterial cellulose production. Biotechnol. Bioprocess Eng. 10(1), 1-8. Biotechnology and Bioprocess Engineering. 10. 1-8. 10.1007/BF02931175.

[13] Sulaeva, I., Henniges, U., Rosenau, T., & Potthast, A. (2015). Bacterial cellulose as a material for wound treatment: Properties and modifications. A review. Biotechnology advances, 33(8), 1547–1571. https://doi.org/10.1016/j.biotechadv.2015.07.009

[14] Trovatti, Eliane & Serafim, Luísa & (Freire, CSR & Silvestre, Armando & Neto, Armando & Neto, Carlos. (2011). Gluconacetobacter sacchari: An efficient bacterial cellulose cell-factory. Carbohydrate Polymers. 86. 10.1016/j.carbpol.2011.06.046.

SYNTHESIS OF COBALT FERRITE NANOPARTICLES IN THE PRESENCE OF ULTRASOUND WAVES AND INVESTIGATION OF THE PROPERTIES OF NANOPARTICLES SYNTHESIZED BY OTHER METHODS

Somayeh Dokhaei, Maedeh Akbari, Yasaman Sanaeirad

ARTICLE INFO

Supervisors: Hamidreza Akbarzadegan

Accepted by Ariaian Young Innovative Minds Institute , AYIMI

http://www.ayimi.org ,info@ayimi.org

ABSTRACT

In this article, we will first review the origin of magnetism in atoms, then the interactions between atoms in a crystal and the origin of these interactions. Then, we will review the general applications of cobalt ferrite nanoparticles and the synthesis of cobalt ferrite in the presence of ultrasound waves, and by comparing different data from numerous articles in this field, we have investigated the effect of various manufacturing methods on the size and properties of cobalt ferrite nanoparticles. Experiments show that the type of manufacturing and synthesis directly affects the size and shape of nanoparticles.

Keywords : *Magnetism, Nanoparticles, Synthesis, Ultrasound waves*

1. Introduction

In this article, we used ultrasound waves to achieve dimensions below ten nanometers. Then, in different nanoparticle samples, we examined the effect of various parameters, including calcination temperature, calcination time, reaction temperature, and baking temperature, on the size and shape and magnetic properties of nanoparticles. On the other hand, it can be said that the size of the particles increases with increasing heat treatment temperature, and this is due to growth in the nanoscale range. Of course, this temperature must be below the melting temperature of the bulk lattice of the material. Superparamagnetism has been reported for cobalt ferrite nanoparticles in the range of 4-10 nm. Also, the results of IR, VSM, and XRD analyses on our prepared sample show that the synthesis method in the presence of ultrasonic waves significantly reduces the particle size, the hysteresis curve reaches zero, and the superparamagnetic property appears.

Magnetic nanoparticles are one of the most important and widely used types of nanomaterials, whose unique properties make them particularly efficient compared to other nanostructures. These particles can be used in various fields. In this article, we prepared a sample of cobalt ferrite nanoparticles (CoFe2O4) using the synthesis method in the presence of ultrasound waves, then compared the magnetic properties of the synthesized sample with other methods. In this article, we have tried to provide general information about cobalt ferrite magnetic nanoparticles, and then specifically examine the achievement of superparamagnetism, which is one of the magnetic properties of nanoparticles, in cobalt ferrite synthesized in the presence of ultrasound waves. It has also been mentioned that cobalt ferrite nanoparticles are one of the most important nanoparticles in the medical and electronics industries and catalysts. First, we will have a brief overview of the origin of magnetism in atoms and introduce the types of magnetic materials by defining them. After that, we present a report on the work done on cobalt ferrite nanoparticles.

2. Origin of Magnetization of Materials

The main carrier of magnetic properties in solids are electrons. In general, the origin of magnetic properties can be considered to be moving electrons. The theory of magnetism is primarily the theory of electronic structure. In ionic crystals, electrons are considered more or less as electrons bound to specific nuclei. At the beginning of the emergence of magnetic theories, many experiments showed that the magnitude of the total angular momentum of an electron and the magnetic moment associated with it are larger than the value attributed to its translational motion. Therefore, an additional contribution resulting from intrinsic properties with one degree of freedom was attributed to the electron and, since this property had the same effect as the rotation of the electron around its axis, it was called spin. Dirac showed that if the equations of quantum mechanics were to be relativistically invariant, there would be a magnitude of angular momentum for the electron. So far, the main origin of the emergence of magnetism, which is the magnitude of the orbital angular momentum and the magnitude of the spin angular momentum, has been considered.

3. Magnetic Phases

Since our activity is in the field of magnetic materials, it is necessary to provide a brief introduction to the types of magnetic materials and the characteristics of each. The most natural way to classify the magnetic properties of materials is to pay attention to their response to an external magnetic field. On this basis, magnetic materials are divided into diamagnetic, paramagnetic, ferromagnetic, antiferromagnetic and ferrimagnetic phases.

3.1. Diamagnetism

Diamagnetism is present in all materials and is a characteristic of all materials and is often covered by stronger magnetizations. Diamagnetic atoms have no magnetic moment and when placed in an external magnetic field, they have an induced magnetic moment in the opposite direction of the external field and weaken it. The magnetic susceptibility of these materials is very small, negative and independent of temperature. Organic materials, light alkaline earth elements, copper, quartz andSiO2 are diamagnetic materials.

3.2. Paramagnetism

The main reason for the paramagnetic property is the presence of unpaired electrons in unfilled shells. A paramagnetic solid is made up of atoms that have

permanent atomic magnetic moments. But they act separately and without any interaction with each other, which ultimately have random orientations due to thermal vibrations. The application of an external magnetic field causes the induced magnetic moments to orient in the direction of the field and strengthen it. However, thermal disturbances cause them to slightly align in the direction of the external field, which results in a small magnetization and magnetic susceptibility. Alkaline earth metals, transition metals and lanthanides are among these.

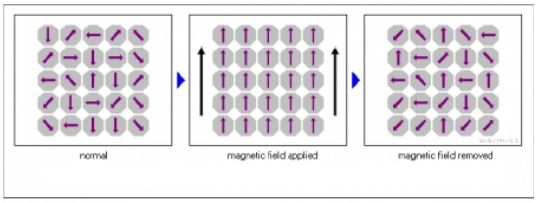

Fig. 1: Paramagnetic

3.3. Ferromagnetism

Ferromagnetism refers to materials that have spontaneous magnetization in the absence of an external magnetic field and, unlike paramagnetism, their magnetic moments interact with each other.

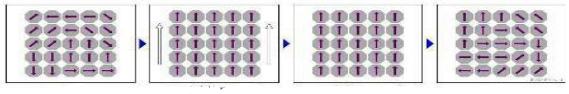

Fig. 2: Ferromagnetic

3.4. Ferrimagnetism

Ferromagnetism is observed only in compounds that have a more complex crystal structure than pure elements and is not observed in pure elements. This condition is also observed in compounds of mixed oxides. Although in these materials the equilibrium interaction causes parallel alignment of magnetic moments in some regions and antiparallel alignment in other regions, the magnitude of their magnetic moments in one direction is greater than the other, and as a result, the net magnetization of the material is not zero and the saturation magnetization of these materials is less than that of ferromagnetism. The magnetic susceptibility of this group of materials is large and positive. Ferrites are prominent examples of ferrimagnetic materials.

3.5. Antiferromagnetism

Antiferromagnetism is formed when a molecular field acts in such a way that the nearest magnetic moments are antiparallel to each other. In antiferromagnet materials, the resulting magnetization is eliminated in the absence of an external field, and in the state of minimum net spin energy, their spin is zero. Often, the crystal lattice of an antiferromagnet is imagined as two intertwined sublattices whose magnetic moments are directed in opposite directions and the molecular field on each sublattice is proportional to the magnetization of the other sublattice. In the periodic table, chromium is the only element that is in the antiferromagnet phase at room temperature. Antiferromagnetism is also found in the transition elements. Manganese oxide, iron oxide, and nickel oxide are examples of antiferromagnet materials.

3.6. Superparamagnetism

Superparamagnetism is a collection of tiny ferromagnetic particles placed in paramagnetic materials, with a distance between them, and this distance is the reason why the moments do not affect each other. When materials that have superparamagnetic properties are affected by an external magnetic field, their magnetic moments align with the field and strengthen it, but in the absence of an external magnetic field, the materials lose this property.

4. Cobalt Ferrite Nanoparticles

In recent years, attention has increased to various magnetic nanoparticles due to their potential for industrial applications. Cobalt ferrite is one of the spinel nanoparticles that has found wide applications in the electronics, medical and catalyst industries due to its strong electrical and magnetic properties, high hardness and magnetic anisotropy, acceptable magnetization and controllable Curie temperature. Cobalt ferrite has wide applications in electronic and magnetic equipment, especially data storage systems. Cobalt ferrite has been used in the core of converters, generators and motors.Cobalt ferrite nanoparticles have wide applications in medical diagnostics. Today, cancer treatment is one of the major challenges due to insufficient precision in surgeries, lack of complete access to the tumor, destructive effects of cancer drugs on healthy tissues in addition to cancer cells, etc., and this has led researchers to seek solutions to these problems. Ferrofluidization of cobalt ferrite nanoparticles is one of the suitable alternatives for cancer treatment. This material is one of the most prominent electroceramics in the field of magnetic and magneto-optical materials, which has developing applications in permanent magnets, magnetic memories, fluids used in medicine, chemical catalysts, magnetocaloric, magnetostrictive, and magneto-optical topics.

5. The Physical and Chemical Properties of Spinel Nanoparticles are Mainly Influenced by the Type and Method of Manufacture and Preparation

As mentioned, cobalt ferrite nanoparticles have a spinel structure. The spinel structure is one of the ternary structures of materials with the general formula AB_2O_4, where A and B are different metal cations. This structure can be considered a combination of the structures of table salt and zinc borate. In the spinel structure, the divalent A ions are located in the tetrahedral holes and the trivalent B ions are located in the octahedral holes.

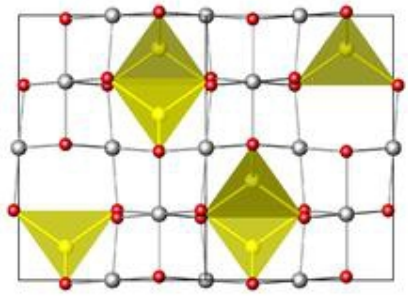

Fig. 3: The spinel structure

5.1. Two Main and Basic Methods are Used to Produce Nanoparticles

1- Physical method (solid phase)

2- Chemical method (liquid and vapor phase)In physical methods, very precise and expensive instruments are mainly required. There are also drawbacks in solid phase

mainly required. There are also drawbacks in solid phase methods, such as the formation of strong bonds in agglomerates, heterogeneity such as undesirable phase, unusual texture growth, poor reproducibility, and inaccurate and imprecise control of cation stoichiometry. For this reason, chemical methods are preferred. Some of these methods include sol-gel, co-precipitation, solvent evaporation, hydrothermal, thermal decomposition, microemulsion, and citrate methods.More chemical methods include successive calcination steps, which causes the nanoparticles to stick together and form agglomerates. On the other hand, it can be said that the presence of different frequencies can affect the size and shape of the particles as well as their magnetic properties. In this article, we have investigated the magnetic properties and size of nanoparticles prepared using the synthesis method in the presence of ultrasound waves and obtained acceptable results.

6. Report on the Work Done on Cobalt Ferrite Nanoparticles

Following, we will review the activities of different people who have studied cobalt ferrite nanoparticles. Different samples of nanoparticles were prepared by different methods and the effect of different parameters, including calcination temperature, calcination time, reaction temperature and baking temperature, on the size and particle size and magnetic properties of the nanoparticles were investigated.

6.1. Effect of Calcination Temperature on Cobalt Ferrite Nanoparticles

In 2004, Juliana Silva and her colleagues investigated the effect of heat treatment of calcination temperature on cobalt ferrite nanoparticles prepared by the co-precipitation method because this method is the simplest and cheapest way to prepare nanoparticles. They used cobalt nitrate and iron nitrate as precursors and ammonia as precipitation agent. On the other hand, the resulting powder required drying and heat treatment steps, which of course caused changes in the magnetic properties and particle size. The result was that with increasing calcination temperature, the particle size and crystal size increased. Spin magnetization also increased with increasing calcination temperature. At 950°C, the particle size increased significantly, which was due to agglomeration and particle adhesion, which caused a rapid decrease in the magnetic coercivity HC from its maximum value to about 0.5. While this temperature is close to the bulk size of 77emu/g.In 2009, Ms. Mehrnaz Gharegozlou prepared cobalt ferrite nanoparticles using the polymer precursor method and investigated the effect of calcination temperature on different samples. In this experiment, aqueous solutions of cobalt and iron nitrate were mixed in aqueous solutions of citric acid and ethylene glycol. This method is based on the immobility of metal ions in the polymer network, while metal cations are homogeneously distributed in the polymer chain. The results of Mehrnaz Gharegozlou's experiments and studies show that with increasing calcination temperature, the particle size increased. The single magnetic domain limit for this sample is 30 nm, where the HC coercivity has reached its maximum value. In general, it can be said that these properties originate from the reduction of particle size in the nano region, the large cross-sectional area, and the change in crystal shape in the interparticle interaction.

In 2001, R.M. Mohammad and his colleagues prepared cobalt ferrite nanoparticles using the organic acid precursor method and investigated the effect of calcination temperature on different samples. In this experiment, he used carboxylic acid both to form a stable complex and as a mobile (energy-generating substance) to increase the reaction temperature during production. The advantages of this method over other methods are the use of cheap raw materials, low reaction temperature, and also a high degree of homogeneity due to the mixing of reactants at molecular levels, which can be easily used in large-scale production. His experimental data also show that with increasing calcination temperature, the spin magnetization increases, and at 1000 ° C, its maximum value is 67.7 emu / g, which is less than the bulk value, and this is due to the large cross-sectional area of the nanoparticles. The difference in the amount of magnetization is probably due to the re-formation and distribution of cations at high temperatures. As in the previous examples, the HC coercivity does not follow a specific pattern with increasing calcination temperature and it can be said that it is not only affected by particle size.

6.2. Effect of Reaction Temperature on Cobalt Ferrite Nanoparticles

In 2006, Yukio Wakyo and his colleagues investigated the effect of reaction temperature on particle size and magnetic properties of cobalt ferrite nanoparticles prepared by co-precipitation method. In this experiment, he used sodium hydroxide, iron chloride and cobalt chloride. His reports of this activity show that with increasing reaction temperature, particle size and average crystal size increase. Significant growth occurred for particles at a temperature of 80 ° C. From which it can be concluded that temperatures above 80 ° C are suitable temperatures for the growth of nanoparticles. At a temperature of 40 ° C, the coercivity value of HC is equal to zero, and in this case we have reached the superparamagnetic property. This point can be understood from the particle size in this temperature range.At higher temperatures, the amount of HC first increases and then decreases. At 80°C, the coercivity of HC is at its highest, which means that a single magnetic domain is formed at this temperature, when the particle size is 34 nm.With increasing reaction temperature, the spin magnetization increases, which is due to the increase in particle size. The maximum magnetization is significantly lower than the bulk value.

6.3. Effect of Annealing Temperature on Cobalt Ferrite Nanoparticles

In 2008, Vinod Kumar and his colleagues investigated the effect of annealing temperature on the size and magnetic properties of cobalt ferrite nanoparticles prepared by co-precipitation. Their results show that with increasing annealing temperature, the size of the nanoparticles and also the average crystal size increase. It can be said that at 1173 ° C, since the HC coercivity has reached its maximum value, a single magnetic domain is created, the size of which for this sample is 35 nm. With increasing annealing temperature, multiple magnetic domains may be created and the HC coercivity decreases because the particle size has increased.

6.4. Effect of Calcination Time on Cobalt Nanoparticles

In 2010, R.M. Mohammad and his colleagues prepared cobalt ferrite nanoparticles using the organic acid precursor method and investigated the effect of calcination

time on different samples. The duration of the calcination process was varied between 0.5 and 2 cm, with the calcination temperature kept constant at 600 °C for three samples. The results are summarized as follows: It can be said that with increasing the duration of the calcination process, the spin magnetization increased and this was due to the increase in particle size, while the HC coercivity decreased.

7. Experimental Section

We prepared a sample of cobalt ferrite using the synthesis method in the presence of ultrasonic waves. Then, we investigated the effect of different parameters during the synthesis process on cobalt ferrite nanoparticles. Among the different methods that could be used to synthesize cobalt ferrite nanoparticles, we used the co-precipitation method because it is the simplest and cheapest way to synthesize nanoparticles. The reason for using ultrasonic waves is to reduce the dimensions of the material to below 10 nm and to develop the superparamagnetic property, which depends on the particle size in the material. To synthesize 3 grams of cobalt ferrite, first 13.5 ml of a solution of M1.88 with respect to iron III and M0.94 with respect to cobalt II was prepared from the relevant nitrites. Then, this solution was rapidly added to 25 ml of a 5.3M solution of sulfur in a glass flask. In the meantime, a mechanical stirrer was also stirring the solution inside the flask. After stirring the solution with a stirrer, we placed it in an ultrasonic device to be exposed to the ultrasonic waves of this device. The ultrasonic device causes changes in the material by introducing a large amount of energy through ultrasonic waves. Among these changes, we can mention the creation of very small bubbles (in nano dimensions) in the solution, the bursting of which breaks the bonds of the solution and rapidly reduces the dimensions. It should be noted that the superparamagnetic property is highly dependent on the particle size and we only see it occur in dimensions of 4-10 nm. After adjusting the pH to 10 and exposing the solution to ultrasonic waves, precipitation was carried out overnight with a 1 molar HCL solution. A portion of this product was baked at an open temperature for 3 hours, which will be referred to as CoR. The other steps, including washing, drying, and baking, were carried out as usual to obtain the CoG sample.

8. Conclusion

According to the above and the preparation of cobalt ferrite nanoparticles using various methods, it can be said that heat treatment and baking or heat treatment time did not affect the structure of cobalt ferrite nanoparticles. These nanoparticles have an extremely strong and stable structure. Different samples of cobalt ferrite nanoparticles have been prepared by various methods under almost equal conditions, the size of the samples is different, which means that the type of manufacturing and synthesis directly affects the size and shape of the nanoparticles. On the other hand, it can be said that with increasing the heat treatment temperature (calcination, baking temperature or reaction temperature), the size of the particles also increases. And this is due to growth in the nano region. Of course, it is below the melting temperature of the bulk lattice. The superparamagnetic limit for cobalt ferrite particles in the nano region has been reported to be between 4 and 10 nm. In this region, the HC range will be zero.The results of IR, VSM, and XRD analyses on our prepared sample show that the synthesis method in the presence of ultrasonic waves causes the hysteresis curve to reach zero and the occurrence of superparamagnetic properties. The results of the analysis of other samples of cobalt ferrite nanoparticles that were synthesized by other methods after baking and after annealing have been examined using IR, VSM, SEM, and XRD. The XRD spectrum shows that the structure of the nanoparticles is spinel. The results from SEM emphasize that the shape of the particles is spherical. VSM data indicate that the resulting particles are ferromagnetic with relatively high anisotropy. Using the IR spectrum, it can be understood that the impurities in the sample are related to the initial nitrate on the surface and between the particles.

References

[1] Peter Mohn. "Magentism in soild state", Springer series in soild state science, 1956.

[2] T.G. Reynolds III, Ferrite magnetic ceramic, in: R.C. Buchanan (Ed.), Ceramics Materials for Electronics, Marcel Dekker, Inc., NY.

[3] S.M. Rezende, A fi´sica de materiais e dispositivos eletroˆnicos, Recife, 1996

[4] Y. Kitamoto, S. Kantake, F. Shirasaki, M. Abe, M. Naoe, J. Appl. Phys. 85(1999) 4708.

[5] M.H. Sousa, F.A. Tourinho, J. Phys. Chem., B 105 (2001) 1168.

[6] Dennis E. Speliotis, J. Magn. Magn. Mater. 193 (1999) 29.

[7] F. Mazaleyrat, L.K. Varga, J. Magn. Mater. 215–216 (2000) 253.

[8] J. Popplewell, L. Sakhnini, J. Magn. Magn. Mater. 149 (1995) 72.

[9] R.S. Molday, D. Mackenzie, J. Immunol. Methods 52 (1982) 353.

DESIGNING THE QUADROCOPTER FOR FAST DELIVERY OF LOADS TO HARDLY ACCESSIBLE PLACES

Pavlov Aleksander Nicolaevitch, Moscow, Russia, warina@yandex.ru

ARTICLE INFO

First place in Izmir IISEEF 2024

Accepted by Ariaian Young Innovative Minds Institute , AYIMI

http://www.ayimi.org ,info@ayimi.org

ABSTRACT

Nowadays, drones play an important role in the lives of people around the world. In this project I offer to use the drone for delivering food or medicines for people during floods and other emergencies. The idea of the project is making a drone which could deliver a first-aid kit and food to hardly accessible places. The drone must have high exactness of delivery, which is achieved by GPS tracking and manual control.

Keywords : *Drone , First-aid kit,* GPS *tracking*, *Manual control*

1. Introduction

Making the quadrocopter model equipped with the release and gripping gear for delivering food or medicines to hardly accessible places is the main goal of this project.

Tasks:

1. Assembling and finding out constructive faults of the experimental frame.
2. Installation of the drone components on the frame, their solder bonding.
3. Setting of electronics.
4. No-load test flight, performance test of the prototype.
5. Lifting capacity test flight.
6. Release and gripping unit assembly.
7. Installation of release and gripping unit on the drone.

2. Methods

Designing, modeling and test work are the methods in this project.

There is the electrical connection of quadrocopter on the figure (1).

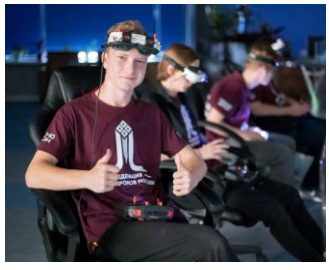

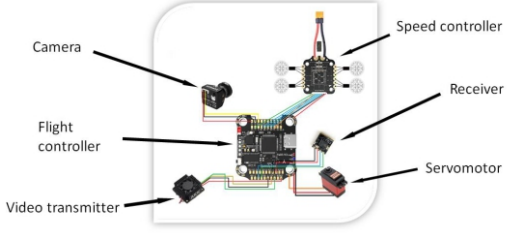

Fig. 1: The electrical connection of quadrocopter

3. Different Parts in Experimental Setup

The Flight controller: is the brain of the drone which all the other components are connected to. Its main task is correct processing of signals from control equipment. The flight controller identifies position of the drone in the air with the help of the installed hygroscope. Vibrations from the motors transmitted to the hygroscope through the frame might interfere with operation, which, in its turn, might lead to loss of control. To avoid this, the controller is placed on vibration isolation.

Electronic speed controller (ESC): controls motors rotation speed. Voltage from the battery is applied on the ESC through power wires. Connection the battery is made through XT60 connector.

The receiver : is the indispensable element of the drone. It receives signals from the control equipment and transmits them to the flight controller.

Camera: is the eye of the drone.

Video transmitter: transmits video from the camera to operator's goggles.

The gripper: is the item which allows to lift and carry different loads. The gripper works with the aid of the servomotor which pushes the piston and closes the lock. The configuration of the gripper that you can see on the first picture appeared to be inefficient because it could not lift a big load. So, the gripper has been redesigned.

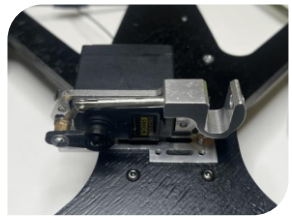

(a) (b)

Fig. 2: a) version 1 and b) Version 2

The frame is the main load bearing element of the drone. The frame should be strong in order not to be deformed

with any physical effect. If one of the frame beams is damaged, the engine wires may be cut by the propeller. That can lead to a shortcut, which, in its turn, might lead to burning of the electronics. The frame was modeled in the CAD program Solid Works (Fig. 3).

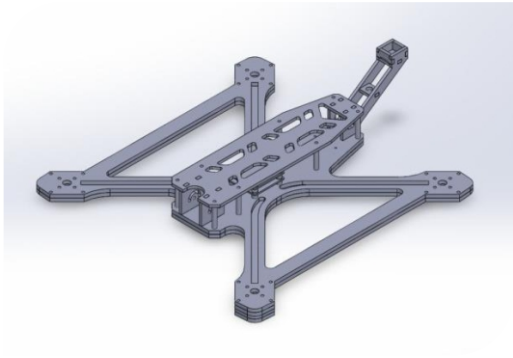

Fig. 3: Frame modeling

It is made of wood, so it is less expensive than carbon fiber. Do not worry about the fact that water can destroy the wood. Firstly, plywood is glued with special adhesives that are not washed away by water. Secondly, the frame is covered with waterproof paint. The weight of the finished model without a battery is six hundred grams. We can use a battery from three thousand milliamps to eight thousand milliamps.

There were a couple of issues during the designing

- There were some problems with coloring the second version of frame, such as sticking to the surface or a bad application of paint to the plywood. Now I know, that I need to color.
- On closing the gripper, the motors stopped. I found out that the trouble originated because the fail save function was set on the same switch with the gripper function by default. As a result, at the moment of closing the gripper, the urgent shutdown of the motors was activated. The problem was solved with setting of the fail save function to another switch.
- The first model of the GPS mount was not suitable in size. The mount was redesigned.

4. Test Results

The drone is in operation, the maximum lifting capacity is 2,5 kilos.

The release and gripping device performs its functions.

Technologies and equipment used:

Soldering equipment including the solder TS100, the laser cutter (Fig. 4).

Fig. 4: The drone in operation

5. Conclusion

During the work, the working quadrocopter model FPV was assembled on the plywood frame. It is capable of lifting the load of 2.5 kilos and equipped with the release and gripping unit (Fig 4).

Prospects of developing the project: to raise the lifting capacity of the gripping unit; providing with an extra thermal camera; making a frame made of a lighter technological material.

Practical use of the project:

- The delivery of first-aid kit and food to hardly accessible places .
- It may be used for delivery of loads under 2.5 kilos.

References

[1] SPEEDYBEE_f405_V3_Manual_EN [Online resource]. URL: https://clck.ru/38vLCg (last accessed date: 18.02.2024).

[2] How to Setup Betaflight VTX Table – SmartAudio Tramp VTX Control [Электронный ресурс]. URL: https://clck.ru/38vLE7 (дата последнего обращения: 18.02.2024).

[3] ExpressLRS module ES900TX/ES900RX Long range ELRS hardware 915mhz/868mhz support instead ES915TX/ES915RX [Электронный ресурс]. URL: https://clck.ru/38vLLj (дата последнего обращения: 18.02.2024).

[4] Russian Airspace Control Order for unmanned aircraft (БВС, БПЛА, ДРОНЫ) [Электронный ресурс]. URL: https://clck.ru/h7KGp (дата последнего обращения: 18.02.2024).

[5] Analysis and Future directions of unmanned aircraft [Электронный ресурс]. URL: https://clck.ru/34RXH4 (дата последнего обращения: 18.02.2024).

[6] Беспилотники меняют деловой мир: кейсы, тренды, перспективы. [Электронный ресурс]. URL: https://clck.ru/38vLd5 (дата последнего обращения: 18.02.2024).

ULTRAHYDROPHOBIC WATER

Sara karami – Farzanegan3

ARTICLE INFO

Supervisors: Hossein Javanmardi

Accepted by Ariaian Young Innovative Minds Institute , AYIMI

http://www.ayimi.org ,info@ayimi.org

ABSTRACT

When a bath filled with soapy water on a vibrator that vibrates vertically maybe a droplet ejected from liquid surface. We explain the droplet behavior experimentally using a loud speaker produces standing waves on a liquid surface. We find the threshold of droplet ejection and different behavior of droplet by changing amplitude and forcing frequency. During these experimental works we found three different behavior that droplet had. So we could assume the droplet behavior and it was same as our experiment.

Keywords : *Soapy water , Droplet on liquid, Standing wave , Ejection droplet , Vibrating bath*

1. Introduction

Heretofore maybe you have observed when a water droplet fell down on liquid surface -actually its water too, it was landing on that for a short period of time. Then it was coalesced with liquid. The behavior of unbounded droplets which are on liquid surface extremely like droplets exude from there and siting on that. In this paper we investigate the bath filled with soapy water on vibrator that oscillates vertically. In this situation maybe drops can exude from liquid surface (Fig.1). Drops illustrate some different behavior on liquid.

Fig.1: May bath vibrates drops can exude from that

Couder et al. [1] have shown a particular state for bouncing droplets. In the vicinity of the Faraday instability, the droplets generate an extended wave _eld on the bath .In 1831; Faraday [2] demonstrated that when a horizontal fluid layer is vibrated vertically, its interface remains flat until a critical acceleration is exceeded. Above this threshold, a field of waves appears at the interface, parametric standing waves oscillating with half the forcing frequency [3-4]. The form of such Faraday waves depends on the container geometry; however, boundary effects can be minimized by using a large container. The Faraday waves have a wavelength prescribed by the relative importance of surface tension and gravity, being capillary and gravity waves in the short and long wavelength limits, respectively. Ultimately, large amplitude forcing leads to surface fracture and the ejection of droplets from the fluid bath. A recent study on the breaking of Faraday waves in a vertically shaken bath has been performed in both the capillary and gravity wave limits by Puthenveettil and Hopfinger [5]. Gravity waves are waves generated in a fluid medium or at the interface between two media when the force of gravity or buoyancy tries to restore equilibrium. An example of such an interface is that between the atmosphere and the ocean, which gives rise to wind waves. When a fluid element is displaced on an interface or internally to a region with a different density, gravity will try to restore it toward equilibrium, resulting in an oscillation about the equilibrium state or wave orbit. A capillary wave is a wave traveling along the phase boundary of a fluid, whose dynamics are dominated by the effects of surface tension. Capillary waves are common in nature, and are often referred to as ripples. The wavelength of capillary waves in water is typically less than a few centimeters, with a speed of 10-20 centimeters/second.

We did experiment with soapy water. This liquid has special structure (Fig.2) that helps us for our experiments.

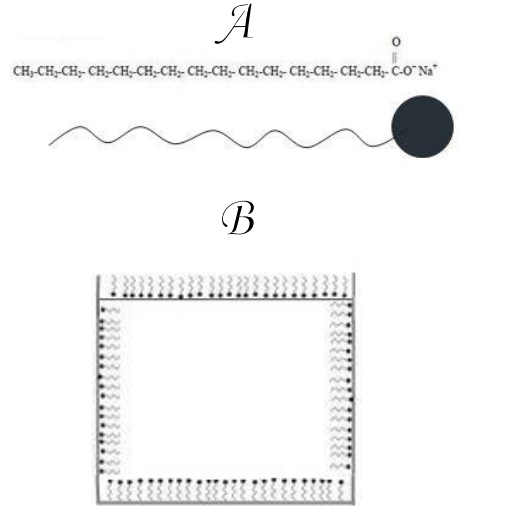

Fig. 2: 'A' is a molecule of soap and 'B' is a bath of soapy water. Afterwards in this paper we survey it

We investigated what happens when a drop of liquid fell down and contact with fluid same with that. Actually we look up what happens wherever occur contact. It was first observed by Lord Rayleigh [6] that the collision of two drops can lead to a rebound, a situation revisited since [7]. The stabilization of drops on the surface of a bulk fluid was first reported by Walker [3] in experiments using vertically

vibrated soap solutions. Several more recent experiments have been concerned with other situations in which coalescence is inhibited [9-10]. Several effects have been shown to delay or inhibit merging. When the interstitial air is forced into flowing, a lubrication effect can generate a lift strong enough to keep the surfaces apart. Other experiments have shown a delayed coalescence in the presence of surfactant [10]. In all these situations the importance of the dynamics of the air layer has been invoked and studied.

2. Methodology

We did experiment with signal generator that produced frequency requirements and it was powered with an amplifier. A container (r=100mm) in different depths of liquid because the depth of liquid is important in different kinds of wave. Actually we changed the viscosity of our liquid with changing value of soap in water. Instead of vibrator we have a loud speaker that oscillates vertically. In our experiment setup (Fig. 3) we used a fast video camera to record our results.

Fig. 3: Experimental Setup

3. Simulation

We simulated the results of other articles in "Ansys workbench .15" (Fig.4). In that simulation we see the first drop ejected from liquid surface in 0.03s.

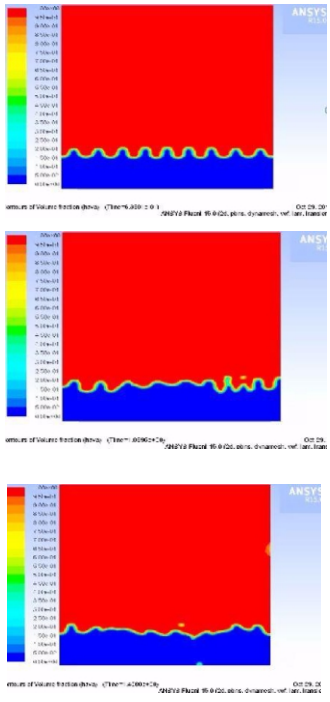

Fig.4: This is "Ansys workbench .15"and the frequency was 100Hz and the amplitude was 0.5mm. The acceleration was 9.8m/s2 and surface tension was 0.7 nm. In this simulation we didn't have cohesion rim.

4. Result

When a drop fell down on liquid surface possibility it illustrates three different behavior: bouncing (Fig.5), staying (Fig.6) and maybe it had walked with bouncing.

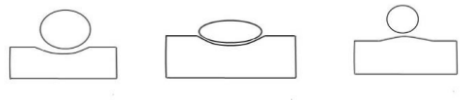

Fig. 5: The drop fell down on liquid surface. The air film between droplet and liquid was squeezed because of the droplet weight. In reaction the air film returned to size that had. After that the drop bounced

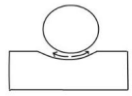

Fig.6: The air film between drop and liquid flowing slowly and for several moments the air inhibition from coalescing and then the drop coalescence with liquid

If we have oscillation bath drops could eject from liquid surface and fell down then landed on that. With each vibrates the air film between drops and liquid is regenerated and this fortuity inhibited from coalesced drops with liquid.

With different frequency and amplitude the air film for different time finished and droplet coalesced. SO We change the frequency and amplitude and contrast condition of ejected droplet in a plot.1 (Fig. 7).

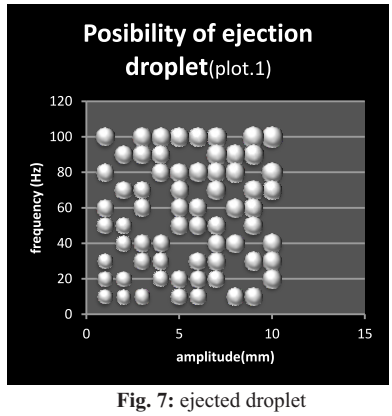

Fig. 7: ejected droplet

As you see in this plot if we increase either forcing frequency or amplitude possibility for ejection droplet increase too. When we increase both of them we have maximum possibility for ejection droplet. Because when we increase forcing frequency the crests of antinodes shrink. ; if the viscosity of our liquid is in low point the possibility again increase. So because of inertia and thin interfacial layer-because of high amplitude- (Fig. 8); the possibility of ejection droplet increase and thereupon the number of droplet increase too.

Fig.8: It's a layer of soapy water between ejection droplet and liquid

In these experiments we saw the size of drop changed. Whereas coalescence because of the weight of drop; we

approximate the size of drop in a plot.2 (Fig. 9).

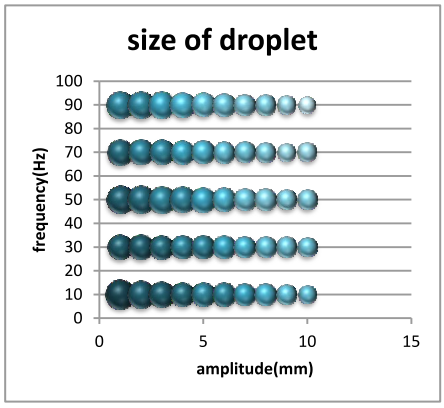

Fig. 9: the size of drop

So the time life of drop on vibrant liquid in high frequency or high amplitude is too longer than in low frequency or amplitude. Thus we understood in high amplitude and frequency both the number of droplet and time life increase.

During all these experiments we got some result about speaker and manner of frequency and amplitude. One of them is very important for our experiments. When the frequency with an amplitude increase the amplitude can`t stay like before. Because of the inertia speaker can't produces same amplitude for high frequency. it's a view of high amplitude and frequency (Fig. 10).

Fig.10: Many droplets excude from liquid

After that all these phenomenon the life time of droplet finish and the drop going to coalescence. The air film between droplet and liquid flowing and after a few seconds its finish. Then before coalescence dependent to percent of soap in water the drop staying on liquid. As if the percent of soap increase the time of staying drop- after finishing the air film -increase too. If amount of soap increase as figure.2 the surface of liquid is compacted (Fig.11). So the weight of drop effect after a few second later.

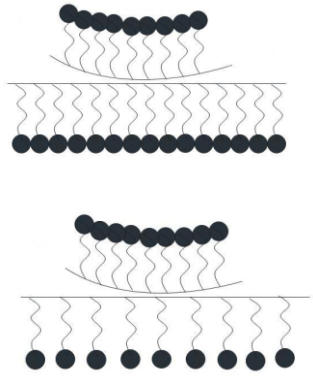

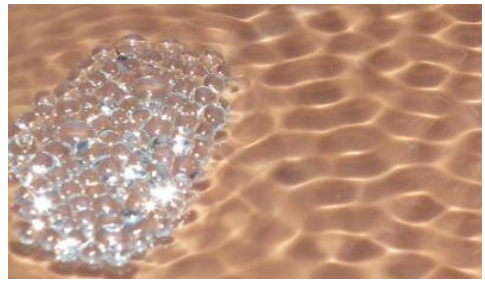

Fig.11: If the surface of liquid is impacted the coalescence happens after a few moments

5. Conclusion

When a bath filled with soapy water on a vibrator that vibrates vertically maybe a droplet ejected from liquid surface. We explain the soapy droplet behavior experimentally using a loud speaker produces standing waves on a liquid surface. We find the drop exude from liquid after 0.03s. If the amplitude and frequency is high and he viscosity is low the number of ejection droplet increase and when the forcing frequency and amplitude in minimum the size of drop is maximum. During these experimental works we found three different behavior that droplet had. When the air film between droplet and liquid squeezed and in reaction the air film wanted returned to size that had the drop bounced. if The air film between drop and liquid flowing slowly; for several moments the air inhibition from coalescing and the drop staying on liquid surface. After these entire phenomenon the life time of droplet finish. Because the air film between droplet and liquid flowing and after a few seconds its finish. . If amount of soap increase the surface of liquid is compacted. So the coalescence happens after a few moments.

References

[1] Y. Couder, S. Protiere, E. Fort and A. Boudaoud, Walking and orbiting droplets, Nature 437, 208 (2005)

[2] Faraday M 1831 On a peculiar class of acoustical figures; and on certain forms assumed by groups of particles upon vibrating elastic surfaces Phil. Trans. R. Soc. Lond. 121 299–340.

[3] Rayleigh L 1883 On the crispations of fluid resting upon a vibrating support Phil. Mag. 16 50

[4] Kudrolli A and Gollub J 1996 Patterns and spatiotemporal chaos in parametrically forced surface waves: A systematic survey at large aspect ratio Physica D 97 133.

[5] Puthenveettil B A and Hopfinger E J 2009 Evolution and breaking of parametrically forced capillary waves in a circular cylinder J. Fluid Mech. 633 355

[6] Lord Rayleigh, Philos. Mag. 48, 321 (1899).

[7] J. Quian and C. K. Law, J. Fluid Mech. 331, 59 (1997).

[8] J. Walker, Sci. Am. 238, No. 6, 123 (1978).

[9] K. R. Sreenivas, P. K. De, and J. H. Arakeri, J. Fluid Mech. 380, 297 (1999).

[10] Y. Amarouchene, G. Cristobal, and H. Kellay, Phys. Rev. Lett. 87, 206104 (2001).

MEASUREMENT OF OXYGEN PRODUCED BY MEAT PLANTS

Zahra Javaheri Tafti, Farzanegan 5, zahra.javaheri.tafti.85@gmail.com

ARTICLE INFO

Supervisors: Rozhin Salmani, Pegahsadat Mirshafiekhozani

Accepted by Ariaian Young Innovative Minds Institute , AYIMI

http://www.ayimi.org ,info@ayimi.org

ABSTRACT

Statistics show that about 5 tons of carbon dioxide is produced annually on the planet, which causes an increase in global temperature and irreparable damage, including the destruction of the ozone layer and the entry of dangerous rays into the Earth's atmosphere, as well as endangering the lives of terrestrial organisms. it is possible. Therefore, the importance of dealing with various methods that can minimize the production of carbon dioxide in the ground, is quite clear. We know that green plants produce carbon dioxide, oxygen and electricity and glucose by consuming. we used very simple tools to understand the amount of oxygen production to use it to help reduce air pollution, etc.

Keywords : *Oxygen, Plant, Carbon Dioxide*

1. Introduction

Plants produce oxygen, glucose and electricity by absorbing carbon dioxide, which helps to reduce air pollution in plants because this absorption of carbon dioxide and oxygen excretion is called plant respiration and that is why plants in Today's world, where we are on the verge of extinction due to factors such as global warming and pollution, causes these factors to decrease because they reduce heat by absorbing carbon dioxide. As we know, carbon dioxide has heat and one of Important factors are global warming.

In this article, we designed 4 ideas, one of which we implemented and continued the article based on it. Our first idea was to use candles and plants, which we have used in this article. The second idea is to use fish. And it was a plant, and our third idea was to use worms and plants. Also, the fourth idea was to use the roots of plants and plants.

In an article by "Norman Henry Harris" the purpose and content of expressing the results, reviews and various quotes from top people and articles in relationship between plant respiration and factors that increase this plant respiration, which was written in "2015" and named "Plant Respiration - Annotated Bibliography" has published.

In an article called "Respiration—that's breathing isn't it?" in the year "1991" by "Jerry Seymour & Bernard Longden" it is written that a research paper (conducted in schools) with the aim of isolating and identifying key concepts in gas exchange and respiration. The results of this study show that the cellular basis of respiration, the nature of respiration in plants is not well understood by students.

In an article called "Thermal acclimation and the dynamic response of plant respiration to temperature" by "Owen K. Atkin, Mark G. Tjoelke"; in year "2003" given the global climate change and the dynamic response of plant respiration with the aim of discussing the basic mechanisms responsible for response plant respiration is subject to temperature changes in the short and long term. The results include the dependence of temperature on the change in control exerted by the maximum enzyme activity at low temperatures and the limitations of the substrate at high temperatures.

An article entitled "Modeling the Components of Plant Respiration: Representation and Realism" by "J. H. M. THORNLEY , M. G. R. CANNELL" in year " 1999" and with the aim of modeling plants it was stated that complete plant models can be formulated in such a way that maintenance or respiration of growth is a priority for the absorbents, or that growth respiration is the difference between total respiration and maintenance along with the synthesis of degraded tissues. During a season and forest respiration during a rotation shows that the ratio of total respiration to photosynthesis of vegetation canopy varies in the predicted limited range. It is also concluded that the growth and respiration maintenance approach, which represents many of the minor processes, is of considerable merit and that parameters still need to be adjusted to make the model predictions acceptable.

In an article entitled "Dry air will change the way plants absorb and breathe in the future" by "Parvin Salehi Shenjani" in "2020" with research on plant respiration and transpiration of plants by its pores came to this conclusion The transpiration and water absorption in plants depends to some extent on factors such as soil and air humidity.

An article entitled "Study of the impact of urban parks on oxygen production" by "Elham Foroutan, Zahra Sadrabadi"; In "2018", with the aim of investigating the amount of oxygen production in urban areas, they realized the result of increasing tree planting to provide oxygen in urban green spaces and is effective in reducing local climate change in the city and cooling the region.

Ms. Maryam Masoom Tamimi in her studies ,"2019", in an article entitled "How do plants work for the earth?" The reaction of plants has increased carbon dioxide and plant respiration. In this article, it has been said that the strength and duration of this reaction is unknown. The result obtained by modeling and analysis is that at the beginning of the industrial age with increasing carbon dioxide. Barley oxide increases the photosynthesis rate of plants in a relatively constant ratio.

In this article, we tried to address the issue of plant respiration to express a solution to measure the amount of oxygen produced in green plants so that we can achieve goals such as reducing carbon dioxide produced by factories and cities and helping to absorb carbon dioxide. More and more oxygen production to clean the air of cities, which of course is possible by measuring the production and consumption of oxygen and carbon dioxide. The other

goals of this article are also related to how to measure and produce oxygen in cities to reduce air pollution and air pollution and make people less exposed to diseases caused by air pollution.

2. Research Method

Ingredients :

2 exactly the same container with a height of 7.9 cm and a diameter of 7 cm at the base

Fleshy plant from the cute flower family has an approximate volume of 4 cubic centimeters

Clay with a volume of 12 cubic centimeters

2 exactly the same container with a height of 8 cm and a diameter of 14 cm and a diameter of 8 cm at the base

2 candles 10 cm high

Two plates 19 and a half centimeters in diameter to cover the compartment (Fig. 1).

Fig. 1: Materials for experiments

3. Experiments

First, we cut the candle in half and lit another candle using a match and poured two or more drops of molten paraffin on the bottom of two glass jars and placed half of a 10 cm candle about 5 cm on them in two fixed dishes. we did. We lit the candles so that according to the height of the glass container and also according to how they are placed in the containers, (they should not be made of plastic in the containers because they melt next to the candle flame.) We kept the candles lit until the height Reached 4.5 cm.(Fig. 2).

Fig. 2: Experiments

Then we put the plant and the mud in the first container and in the second container we put the same amount of mud so that the conditions are the same for both and the only variable in this comparative experiment was the presence or absence of the plant in the containers.

We lit them with a matchstick. In this experiment, the equality of the flames as well as the light and the location of the dishes are among the effective points in the result of the experiment, so we repeated the point of equality of the flames during the repetition of the experiment. We waited for 1.5 seconds for the flames to be the same size. We started the experiment and after lighting the candles and comparing the flame equality of the candles, we placed the doors on the dishes at the same time so that no gas entered the dishes and we observed that the second dish was turned off earlier than the first dish. We repeated the experiment. The second time was the same as the first time, but because the time of placing the doors was not the same and we had placed the second container earlier, the candle in the second container was extinguished sooner.

Fig. 3: Steps 1 and 2

We repeated the experiment for the third time, the length of the candles was shorter, but the important point was that when the candle of the first container was shorter than the candle of the second container, we lit the candle of the second container to be the same size as the candle of the first container. In the third time, we observed that the candle in the first container containing the plant was extinguished earlier.

We repeated the experiment for the fourth time and saw that the candle in the second container was extinguished earlier than the candle in the first container that contained the plant. The fifth time, the candle in the first container with the plant was extinguished later than the candle in the second container, and this time difference was in 1 second and 26 hundredths of a second. In the sixth time, we obtained the same result, with the difference that this time the candle was extinguished earlier in the second time, 1 second and 41 hundredths of a second earlier (Table 1). Flame, temperature, etc. We were careful (Figs. 4 and 5).

Fig. 4: Steps 4, 5 and 6

Fig. 5: Steps 4,5 and 6

We repeated the experiment again using the same plant and the same mud and candles, but this time in a larger container with a height of 8 cm and a diameter of 14 cm and a diameter of 8 cm. We repeated 4 times. As before, separate the candles from the previous dishes and fix the candle with the same size of 3.5 cm using melted paraffin

drops in the same place of the dishes and repeat the experiment as before (Fig. 6).

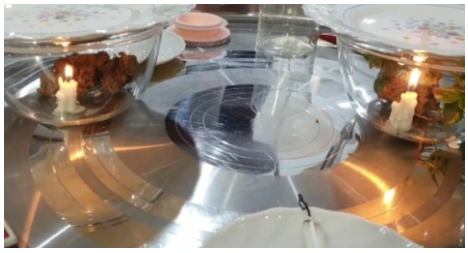

Fig. 6: The other kind of dishes

In the first time, an error such as not placing the containers at the same time caused us not to divorce the experiment properly because the conditions must be the same, so we repeated the experiment for the second and third time, and the result was the second time that the container had plants. It was turned off earlier than the other container, but in the third and fourth times, the container that did not have a plant was turned off earlier than the container that had a plant, and in the fifth time, the time difference was 2.16 seconds. The same result was obtained in the sixth time, with the difference that the container without the plant was turned off for 2.62 seconds of a second earlier. (Table 2).

Table 1: First kind

Times repeat experiment	first container(with plant)went out	second container(without plant)went out
first time		*
second time		*
third time	*	
Forth time		*
fifth time		* With a time difference of 1 seconds and 26 hundredths of a second
Sixth time		* With a time difference of 1 seconds and 41 hundredths of a second

Table 2: Second Kind

times repeat experiment	first container(with plant)went out	Second container(without plant)went out
first time	*	
second time	*	
third time		*
forth time		*
fifth time		* With a time difference of 2 seconds and 16 hundredths of a second
sixth time		* With a time difference of seconds and hundredths of a 62 second

So we noticed that in the second container, due to the lack of plants, the spark plug had lost its fuel, which is actually oxygen. In the first container in which the plant was placed, since we know that the volume of oxygen and gases in the two containers was the same in the beginning, so the presence of the plant caused the plant to breathe and this respiration caused the absorption of carbon dioxide. And oxygen was produced. This produced oxygen caused the candle in the first container to lose its fuel later than the candle in the second container, and in this way it can be understood how much oxygen the plant produced in the first container, which caused this result. If you look closely, you will see that the volume of the containers in each of the two types of experiments is exactly the same as the two containers, and they were the same in all four containers. In a container in which the plant was not present, because the candle was extinguished earlier, it indicates that the container containing the plant had produced as much oxygen as the volume of the container itself.

4. Analysis and Conclusion

The result obtained from the experiment shows that according to the volume of the container, the amount of oxygen production in the plant changes and the plant can consume different volumes of carbon dioxide and produce oxygen. He had filled the entire volume of the container with carbon dioxide and consumed all the oxygen in the container. Therefore, it can be said that due to the comparability of the experiments, when the volume of the first container is filled with carbon dioxide, the plant absorbs carbon dioxide and produces glucose and oxygen. As we have seen, in the first type, when the volume of the containers was smaller, the candles collapsed earlier and with less time difference, so we understand that the amount of carbon dioxide production of the candle as well as the amount of plant oxygen production are our variables.

In this experiment, we found that using the volume formula, in the first type, the volume of oxygen produced is 303.8735 and in the second type, the volume of oxygen produced is approximately 628 cubic centimeters.

In our opinion, this experiment has been done well due to the existence of conditions such as the following. .. It is good for us to get the result, but this issue still needs to be researched.

According to the article written by "Maryam Masoumi Tamimi" which is mentioned in section 10 of the research background, we came to the conclusion that the reason for the same results that with increasing carbon dioxide production also increases oxygen production because we also increase the volume of our container, carbon. More carbon dioxide was produced by the candles, and more oxygen was produced in the container where the plant was because the candles were extinguished later than the first type.

References

[1] Theodorou, Maria E., and William C. Plaxton. "Metabolic adaptations of plant respiration to nutritional phosphate deprivation." Plant physiology 101.2 (1993): 339-344.

[2] Harris, Norman Henry. "Plant Respiration-Annotated Bibliography." (2015).

[3] Atkin, Owen K., and Mark G. Tjoelker. "Thermal acclimation and the dynamic response of plantrespiration to temperature." Trends in plant science 8.7 (2003): 343 -351.

[4] Plaxton, William C., and Florencio E. Podest · "The functional organization and control of plantrespiration." Critical Reviews in Plant Sciences 25.2 (2006): 159-198.

[5] Ryan, Michael G. "Effects of climate change on plant respiration." Ecological Applications 1.2 (1999 157-167.

[6] Smith, Nicholas G., and Jeffrey S. Dukes. "Plant respiration and photosynthesis in global-scalemodels: incorporating acclimation to temperature and CO 2." Global change biology 19.1 (2013): 45-63.

[7] Thornley, J. H. M., and M. G. R. Cannell. "Modelling the components of plant respiration: representation and realism." Annals of Botany 85.

[8] Pilon-Smits, Elizabeth, and Marinus Pilon. "Breeding mercury-breathing plants for environmentalcleanup." Trends in Plant Science 5.6 (2000): 235-236

[9] Arlander, Annette. "Breathing and Growth: Performing with plants." Journal of Dance & SomaticPractices 10.2 (2018): 175-187.

[10] Seymour, Jerry, and Bernard Longden. "Respiration—that's breathing isn't it?." Journal of Biological Education 25.3 (1991): 177-183.

[11] Moar, William J. "Breathing new life into insect-resistant plants." Nature biotechnology 21.10 (2003): 1152-1154.

[12] Pirone, Pascal P. Diseases and pests of ornamental plants. John Wiley & Sons, 1978.

[13] Vince-Prue, Daphne. "Photoperiodism in plants." (1975).

[14] Markert, Bernd. "Plants as biomonitors." (1993).

[15] Kendrick, Richard E., and Gerd HM Kronenberg, eds. Photomorphogenesis in plants. Springer Science & Business Media, 2012.

[16] Diaz, Edgar A., et al. "Toxicological evaluation of realistic emission source aerosols (TERESA)—power plant studies: assessment of breathing pattern." Inhalation toxicology 23.sup2 (2011): 42-59.

[17] Pilon-Smits, Elizabeth, and Marinus Pilon. "Breeding mercury-breathing plants for environmental cleanup." Trends in Plant Science 5.6 (2000): 235-236.

[18] Cherniack, Neil S., and Guy S. Longobardo. "Mathematical models of periodic breathing and their usefulness in understanding cardiovascular and respiratory disorders." Experimental physiology 91.2 (2006): 295-305.

[19] Malek, R. F., J. M. Daisy, and B. S. Cohen. "Breathing zone concentration variations in the reinforced plastic industry; Field measurements in a boat manufacturing plant." Applied occupational and environmental hygiene 14.11 (1999): 777-784.

HOLD ON TO LIFE

Cemre Coskun, Akın Atabulu, Kaan Efe Ibis, Muhammet Coruh , Eraslan High , muhammet.coruh@eraslan.k12.tr

ARTICLE INFO

First Place in Izmir IISEEF 2024

Accepted by Ariaian Young Innovative Minds Institute , AYIMI

http://www.ayimi.org ,info@ayimi.org

ABSTRACT

Turkey is located on active fault lines with the potential to produce high-magnitude earthquakes. This reality highlights the need for all of us to live with the constant awareness of earthquakes. With preventive measures before a disaster and intervention plans implemented afterward, it is possible to minimize losses from major earthquake disasters. To prevent similar challenges in future earthquakes, a system is being developed that would allow people trapped under rubble to send signals to rescue teams. This project proposes the design of a bracelet intended to facilitate the rescue of individuals trapped under debris after a disaster.

Keywords : *Earthquake, Signals, Bracelet, Rescue*

1. Introduction

Natural disasters are natural phenomena that are mostly beyond the control of individuals, and the lack of necessary precautions often leads to significant loss of life and property during such events (Kutluay, 2017). Globally, the most frequently experienced natural disasters are floods, extreme weather events, and earthquakes (Our World in Data, 2020). Earthquakes cause the most significant loss of life and property, and Turkey is among the countries that experience the highest casualties and damages due to high-magnitude earthquakes (Hastürk & Altan, 2023).

The response phase becomes particularly critical after a disaster occurs. Rescuing individuals trapped under rubble following an earthquake is a race against time. While most rescues happen within the first 24 hours, the first 72 hours, often referred to as the "golden hours," are crucial for rescue operations (Huo et al., 2011). To conduct search and rescue operations swiftly and efficiently, it is vital to accurately determine the number of people trapped under the debris, their condition (whether they are alive), and their exact locations within the debris. Based on this information, search and rescue teams can allocate their limited equipment and personnel resources within the constrained timeframe to the most critical areas, enabling them to create the most efficient operational plan (Öztürk & Bayır, 2023).

Various methods are used in search and rescue operations. Since each method has its own advantages and disadvantages, a combination of multiple methods is typically employed (Şahin, 2019).

If individuals trapped under debris after an earthquake can send a signal to indicate their location to search and rescue teams, the teams can obtain more accurate information about the number of people under the rubble, their survival status, and their exact locations. This would enable search and rescue operations to be managed with greater efficiency.

This study aims to develop a low-cost bracelet compatible with sensors currently used in search and rescue operations. The bracelet is designed to facilitate search and rescue activities for individuals trapped under rubble or debris following a potential disaster, help them make their voices heard by rescue teams, and provide psychological comfort to those trapped beneath the debris.

2. Methodology

The design of the bracelet was created using the Tinkercad software (Fig.1). The initial circuit included a pulse sensor, a buzzer, an RGB LED, and an Arduino Uno. The programming phase of the application was completed using the Arduino programming language. After assembling the prototype circuit, the code was uploaded, and the circuit was tested. During the tests, it was observed that the buzzer was insufficient, and a three-legged buzzer sound card was chosen for replacement. Subsequently, the circuit was miniaturized using an Arduino Pro Mini (Fig.2). Additionally, a Type-C connection was added to the circuit for battery charging. As the final step in the circuit design, a vibration motor was integrated into the system (Fig. 3). To ensure that search and rescue teams can quickly and reliably access the necessary information, a QR code containing the user's personal information was placed on the back of the bracelet.

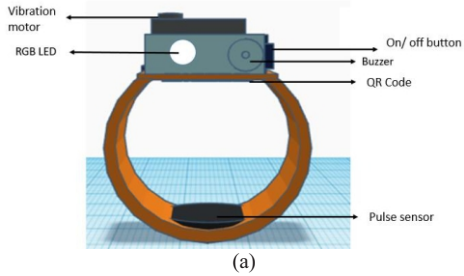

(a)

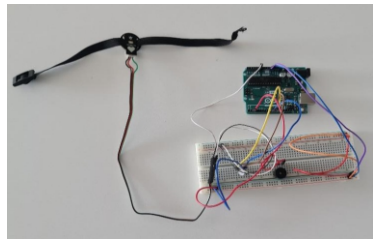

(b)

Fig.1: a) The bracelet design drawn in the Tinkercad program , b)The first circuit of the bracelet

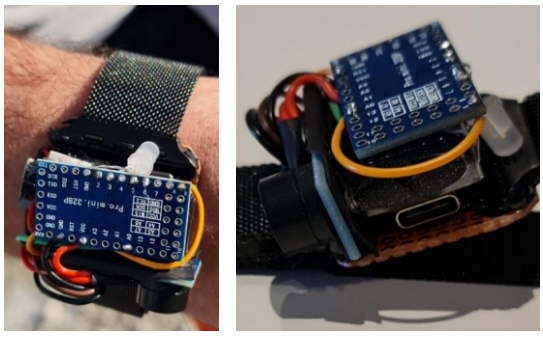

Fig. 2: Reducing the circuit size using the Arduino Pro Mini (left), Type-C connection (right)

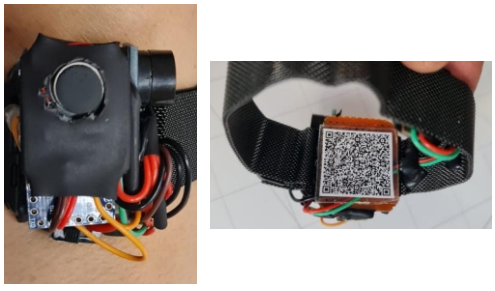

Fig. 3: The vibration motor integrated into the circuit (left), the QR code located on the bottom of the bracelet (right)

In the final stage, the effectiveness of the earthquake bracelet and its delectability by sound-listening devices used by search and rescue teams were tested with support from the Izmir Disaster and Emergency Management Authority (AFAD). The first test involved placing the bracelet near two sensors and then moving it closer to one of them (Fig. 4). For the debris test, three sound detection sensors were placed on the debris, connected to a listening device (Fig. 5). A search and rescue team member wore the bracelet and went under the debris, where they activated it. Another team member then monitored the sound frequencies from the bracelet using the listening device.

Fig. 4: Placing the bracelet between the two sensors (left), bringing the bracelet closer to one of the sensors (right)

Fig. 5: Image from the test conducted under the debris

3. Results and Discussion

The "earthquake bracelet" developed in this study activates when the user switches it on during an earthquake. Once activated, the pulse sensor on the bracelet monitors the wearer's heartbeat. If a pulse is detected, the device emits a high-pitched C note (523 Hz) for 30 seconds every minute, illuminates a blue LED light, and activates the vibration motor (Fig. 6). If no pulse is detected, the device emits a low-pitched C note (262 Hz) for 30 seconds every two minutes and illuminates a red LED light. This system enables search and rescue teams working on-site to accurately determine the number of living or deceased individuals under the rubble, facilitating the creation of a rapid and efficient rescue plan based on this information.

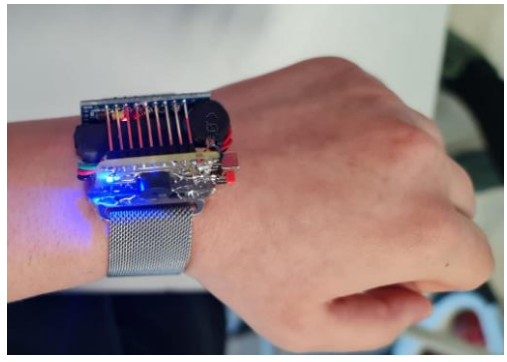

Fig. 6: Testing of the bracelet by users

During the evaluation of the bracelet's effectiveness under debris, it was determined that the sound emitted by the bracelet is audible to the naked ear when operating beneath debris. Additionally, the sound was successfully detected by listening devices. The vibration waves produced by the bracelet were also effectively identified by these devices. Tests conducted under debris confirmed that the signals from the bracelet could reach the surface and be recognized by sound detection devices. In earthquake scenarios, potential issues such as power outages and disruptions to mobile phone networks are common. Therefore, this study ensured that the device operates independently of electricity and mobile network systems to prevent such issues.

By sending different signals based on whether individuals trapped under the rubble are alive or deceased, the bracelet serves as a critical guide for search and rescue teams, helping them allocate their limited resources and manpower more effectively.

Various technological products are being developed to support search and rescue activities after a disaster. One such study proposed a device in an earthquake bag that communicates with search teams via IoT (Öztürk & Bayır, 2023). However, people who cannot carry the earthquake bag during the earthquake would be left without assistance, limiting the device's use. In contrast, the bracelet developed in this study can be worn by anyone throughout the day and used regardless of where they are when the earthquake occurs. Another study suggested using a robotic explorer inspired by reptiles to gather information about rubble (Kedikli et al., 2022). However, such robots are expensive and limited in number, so their efficiency would be improved when used in combination with the bracelet signals for more targeted searches. Similarly, a study by Öztürk and Palay (2023) developed a sound-processing system to accurately locate sound sources under rubble. In our study, the earthquake bracelet can work alongside such systems to quickly and accurately identify the location of trapped people, distinguishing between living and deceased, thus speeding up interventions.

Considering the feasibility and ease of use of the work, it can be said that an innovative product has been created. Based on users' demands, the bracelets can be produced in different colors, patterns, and sizes, suitable for all ages

and in accordance with fashion. In this way, a bracelet that is worn 24/7 and provides an opportunity for rescue teams to reach people during any disaster can be used by everyone .

References

[1] Hastürk, O., & Altan, M. F. (2023). Depremin Ardından Kentsel Dönüşüm. Avrasya Dosyası, 14(1), 146-170.

[2] Huo, R., Agapiou, A., Bocos-Bintintan, V., Brown, L. J., Burns, C., Creaser, C. S., ... & Thomas, C. L. P. (2011).

[3] The trapped human experiment. Journal of breath research, 5(4), 046006.

[4] Kedikli, K., Yıldız, B., Toka, K., & Genç, A. (2022). Performing of Reptile Robot Prototype with Radio Frequency Remote Control for the Exploration After the Earthquake Ruins. Gazi Journal of Engineering Sciences (GJES), 8(1), 41-48.

[5] Kutluay, H. (2017). Doğal Afet Nedir, Çeşitleri Nelerdir? Available from: https://www.makaleler.com/dogal -afetler-nelerdir. (15 Dec 2023).

[6] Our World in Data. (2020). Global reported natural disasters by type. Available from: https://ourworldindata.org/grapher/naturaldisasters-by -type. (17 Dec 2023).

[7] Öztürk, İ., & Bayır, B. (2023). Deprem Sonrası Enkaz Altındaki Canlıların Tespiti ve Konumlandırması için IoT Çözümü. M. Öztürk, M. Kırca (Ed.), Kahramanmaraş Merkezli Depremler Sonrası için Akademik Öneriler içinde (483-492. Ss). İstanbul: Özgür Yayın Dağıtım.

[8] Öztürk, İ., & Payal, E. (2023). Ses İşleme Destekli Deprem Sonrası Enkaz Altında Mahsur Kalan Canlılar için Konumlandırma Sistemi. M. Öztürk, M. Kırca (Ed.), Kahramanmaraş Merkezli Depremler Sonrası için Akademik Öneriler içinde (493-502. Ss). İstanbul: Özgür Yayın Dağıtım.

[9] Şahin, Ş. (2019). Türkiye'de afet yönetimi ve 2023 hedefleri. Türk Deprem Araştırma Dergisi, 1(2), 180-196.

WATER WAVES

Maryam shahrami , Farzanegan 3 School

ARTICLE INFO

Supervisors: Hossein Javanmardi

PYPT national tournament

Accepted by Ariaian Young Innovative Minds Institute , AYIMI

http://www.ayimi.org ,info@ayimi.org

ABSTRACT

In this paper, oscillation of the horizontal cylinder on the surface of the water, vortexes and water waves on the surface were investigated. Till now in different articles, different shapes of the floater and Viscosity of the liquid has been studied. But In this article the parameters that depends on the cylinder`s shape, vortexes and some parameters like (frequency, amplitude and etc.) have been surveyed. In our experiments we saw that under certain conditions, the water waves drift away from or toward the floater (cylinder). Motion of the water is different than the motion of the wave. Water at each location moves in a circular Path, but the motions at different locations are "out of phase".

Keywords : *Cylinder, Amplitude, Frequency, Drift away, Circular path*

1. Introduction

When we generate water waves in a horizontal cylinder, different shapes of water waves and vortex are created on the surface of the water and the waves drift away or toward from the cylinder. In different research papers they changed the geometrical parameters of the shape of the floater and viscosity of the liquid and got some results. Now we did some investigations according to their works. We did some experiments to see what will happen and changed the parameters affecting on this phenomenon.

In fact Water waves are the waves having two types: "Gravity waves and Capillary waves" .

Gravity waves are waves generated in a fluid medium or at the interface between two media when the force of gravity or buoyancy tries to restore equilibrium. An example of such an interface is that between the atmosphere and the ocean, which gives rise to wind waves. When a fluid element is displaced on an interface or internally to a region with a different density, gravity will try to restore it toward equilibrium, resulting in an oscillation about the equilibrium state or wave orbit.

A capillary wave is a wave traveling along the phase boundary of a fluid, whose dynamics are dominated by the effects of surface tension. Capillary waves are common in nature, and are often referred to as ripples. The wavelength of capillary waves in water is typically less than a few centimeters, with a speed of 10-20 centimeters/second.

Also other types of waves are "Faraday waves and Plane waves".

Faraday waves, also known as Faraday ripples, are nonlinear standing waves that appear on liquids enclosed by a vibrating receptacle.

Plane waves are constant-frequency waves whose wave fronts (surfaces of constant phase) are infinite parallel planes of constant peak-to-peak amplitude normal to the phase velocity vector.

They are linear waves but when we change amplitude they change to non-linear 3D waves.

2. Methodology

Our solving method was doing some experiments and changing parameters that depend on this problem, like length of the cylinder, frequency, amplitude, viscosity of liquid, material of the cylinder, density of liquid, height of the water, diameter of the container and surface tension. Some parameters like viscosity of the liquid, material of the cylinder, density of liquid were constant.

The experimental setup was made of a big container (in diameter of 2meter) , particles to see the direction of the waves , cylinder and speaker used as a vibrator (Fig.1) .

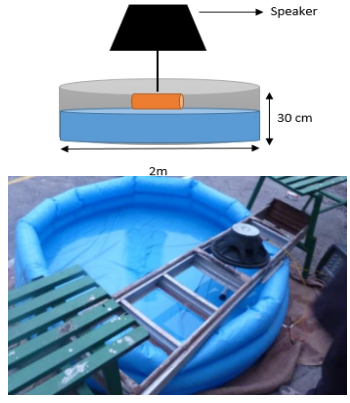

Fig. 1: Experiments setup

The effect of the diameter of the container: if it isn't big enough the waves strike to the container's walls and it affects on waves not to be standing waves. Also height is effective on waves. The distinction between deep and shallow water waves has nothing to do with absolute water depth. It is determined by the ratio of the water's depth to the wavelength of the wave.

The size and weight of the particles (Styrofoam) are important according to the amplitude and wavelength which they moved by. Actually we need different amplitudes and frequency to move particles.

Fig.2: particles

3. Theory

As we said Motion of the water is different than the motion of the wave. Water at each location moves in a circular path, but the motions at different locations are out of phase which means when water at the left of the diagram is moving to the right, water a quarter of a wavelength to the right is moving down, and water next to it is moving to the left, and next to it is moving up, etc (Fig. 3).

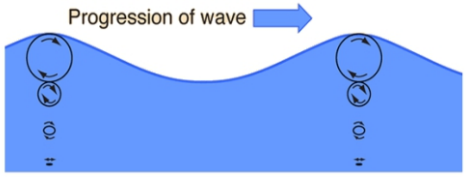

Fig.3: Difference between waters motion and wave`s motion

The overall moving is an apparent wave moving to the right. Thus, the velocity (speed) of a wave is not at all the same as the velocity of the water.

The experimental wave shape is described as a "trochoid". A trochoid can be defined as the curve traced out by a point on a circle as the circle is rolled along a line (Fig. 4).

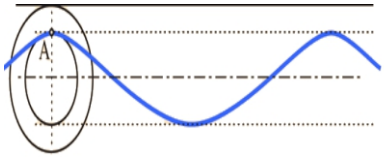

Fig. 4: Trochoid

The discovery of the trochoidal shape came from observation that particles in the water would execute a circular motion as a wave passed without significant net advance in their position.

The water molecules of a deep-water wave move in a circular orbit. The diameter of the orbit decreases with the distance from the surface (Fig.5). The motion is felt down to a distance of approximately one wavelength, where the wave's energy becomes negligible.

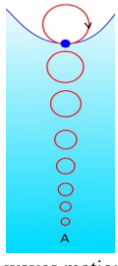

Fig.5: water waves motion (deep water)

The orbits of molecule of shallow water waves are more elliptical (Fig.6).

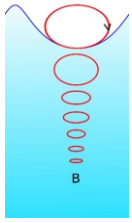

Fig.6: water waves motion (shallow water)

The change from deep to shallow water waves occurs when the depth of the water, d, becomes less than one half of the wavelength of the wave one half of the wavelength of the wave, λ. When d is much greater than λ/2 we have a deep-water wave or a short wave .When d is much less than λ/2 we have a shallow-water wave or a long wave.

Their wave speeds increase with wavelength, a behavior that is called "normal dispersion". For waves shorter than 1.73 cm, the surface tension of the water exerts a controlling force they are "capillary waves". Their speed increases as the wavelength gets shorter, a behavior that is called "anomalous dispersion". The minimum wave speed at wavelength 1.73 cm is 23.1 cm/s.

4. Results of Experiments

We did experiments and changed some parameters like amplitude, frequency, length of the cylinder.

Also we changed the particles` size and the number to know the direction of the vortices.

In our experiments we understood that: Trajectories of fluid particles on the surface were described analytically only for progressing small amplitude planar waves, where particles move in the direction of wave propagation, along the prolate trochoid (Figs.7 and 8).

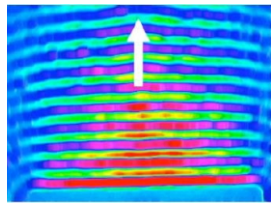

Fig.7 : Plane waves (direction of wave propagation)

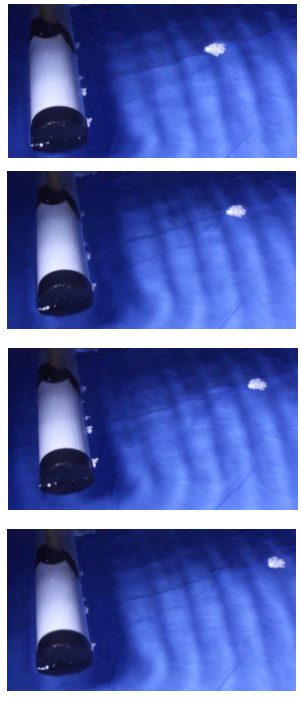

Fig.8: Moving particles in the direction of wave propagation

When we use an elongated cylinder, propagating waves have oval shape and the wave fronts are modulated even at relativity low amplitude.

The maximum of the wave amplitude is at the center of the cylinder side here, floating particles are pushed in the direction of the wave propagation forming strong outward

jet (Fig.9).

Fig.9 : Maximum of the wave amplitude

The flow changes dramatically when the wave amplitude is increased above the modulation.

Instability threshold at only 20-30% higher acceleration of the wave maker (cylinder).As the modulation grows and the cross wave instability breaks the wave front into the trains of propagating wave pulses, the wave field becomes 3D (Fig.10) .

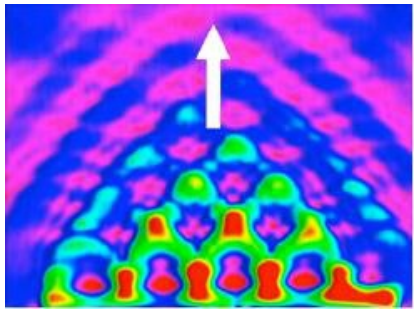

Fig.10: As the wave maker acceleration is increased (30%) the modulation instability destroys the wave planarity generating 3D wave field shown here

Simultaneously, the direction of the central jet reverses. It now pushes floaters inward, towards the wave maker and against the wave propagation! The flow is strong enough to move small objects on the water surface, for example a ping pong ball or Styrofoam (Fig.11).

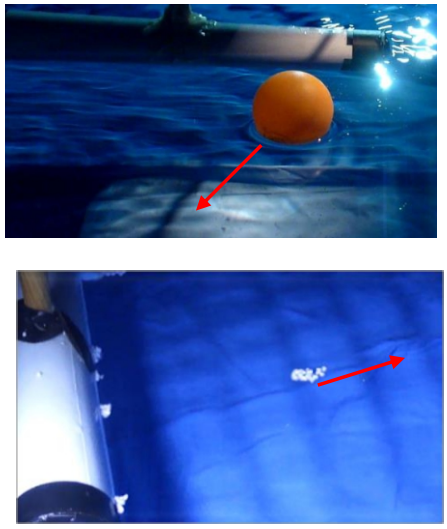

Fig.11: Strong flow on the surface

We find that these waves are produced by the nonlinear 3D waves in the range from long gravity waves (8Hz) to short capillary waves (50Hz).

A quadruple pattern made of 4 large counter-rotating vortices .A quadruple pattern is formed around the cylinder made of 4counter-rotating vortices. Two jets develop in the direction away from the wave maker (Fig.12).

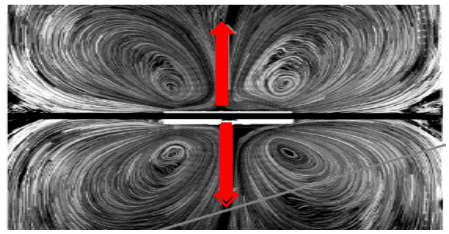

Fig.12: a quadruple pattern is formed around the cylinder made of 4 counter-rotating vortices. Two jets develop in the direction away from the wave maker

The direction of the vortex rotation however reverses with the increase of modulation .This reversal at higher wave amplitudes is always correlated with the generation of stochastic Lagrangian trajectories within a flow region in front of the wave maker (Fig.13) .This complex chaotic flow efficiently transports fluid in the direction perpendicular to the propagation of the wave pulses.

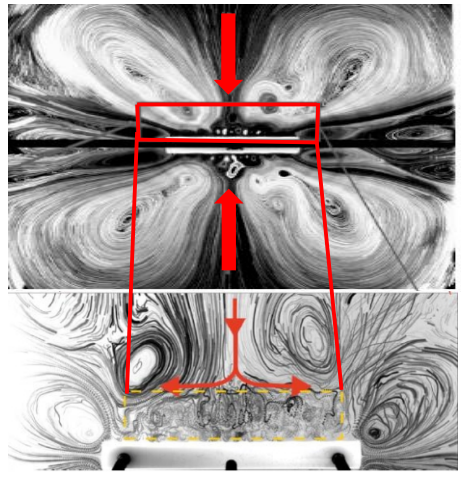

Fig.13. Particle streaks in the vicinity of the cylindrical wave maker visualize a region of Lagrangian stochastic transport (yellow dashed box).Turbulence pumps particles away in the direction of red arrows, orthogonal to the wave propagation

Actually at higher amplitudes particles absorb to the cylinder and at lower amplitudes they drift away the cylinder. In fact we can say that the frequency moves the waves in their direction but amplitude changes their direction.

Frequency is independent of the movement of the particles (direction of the wave`s movement.)

After specific frequency we cannot have the same amplitude like before, because of the inertia force of the speaker. And we can`t see the changes in the direction of the waves after this. It means that when we increase the frequency, amplitude decreases.

5. Conclusion

The investigation was about the surface waves that are created by a cylinder on the water in the vessel . In our method we changed some parameters like amplitude, frequency, length of the cylinder and etc.

A particle is moving in a circular way, but it doesn't have

a vector the same as other particles (actually the molecules doesn't traverse same ways). So it causes the movement in different directions.

If the amplitude and frequency be constant the water molecules travers their circular way completely, but when we increase them their speed goes up and they don't have time to travers all the directions and as a result we see that they go up and down and throw out and get different shapes.

We understood that frequency isn't effective on the drifting away of the waves and it's the effect of amplitude. Also the travers direction of molecules depend on the depth of the water.

References

[1] N. Francois, H. Xia, H. Punzmann, S. Ramsden, and M. Shats. Three-Dimensional Fluid Motion in Faraday Waves: Creation of Vorticity and Generation of Two Dimensional Turbulence. Phys. Rev. X 4, 021021 (2014).

[2] H. Punzmann, N. Francois, H. Xia, G. Falkovich, and M. Shats. Tractor beam on water surface (2014).

[3] H. Punzmann, N. Francois, H. Xia, G. Falkovich, and M. Shats. Generation and reversal of surface flows by propagating waves. Nature Physics 10, 658–663 (2014).

[4] S. Taneda. Visual observations of the flow around a half submerged oscillating circular cylinder. Fluid Dyn. Research 13, 119–151 (1994).

[5] Physicists create water tractor beam (phys.org, August 10, 2014)

SALT PRODUCTION

Sara Ghaderi , Farzanegan 2 School

ARTICLE INFO

Supervisors: Mohammad Qorbani

PYNT national tournament 2017

Accepted by Ariaian Young Innovative Minds Institute , AYIMI

http://www.ayimi.org ,info@ayimi.org

ABSTRACT

Here, four extremely useful simple methods are showed to extract salt (pure NaCl) out of natural sources. These methods don`t need special equipment and can be used easily, even for small amount and at home. Extracted salt, is enough healthy to eat. Methods involve: the sponge using method, plain evaporation, microwave and magnifying glass. Optical microscope was used to study salt crystals formation. Purity of the product and capacity of the methods were investigated.

Keywords : *Natural source, (NaCl), Extracted salt, Plain Evaporation*

1. Introduction

Sodium chloride is the chemical name for salt [1]. Salt is an important material in living system (our body) and in industrial aspects. It can provide useful ions to increase the performances of our muscles and besides making food delicious, it's believed there are more than 14,000 uses for salt [2]. The ancient Egyptians, Greeks and Romans invoked their gods with offerings of salt and water and some people think this to be the origin of Holy Water in the Christian faith .

Table salt is mostly extracted by these three methods: (I) solar evaporation, (II) Thermal evaporation, and (III) rock mining [3]. In solar evaporation, Salt water is captured in shallow ponds and allowed to evaporate by means of the sun and wind [4]. Solar method is the oldest way which can sometimes cause infectious disease. This solar evaporation needs special clime in short duration of time. Although in some places residual salt from dried Salinas are purred and used as eating salt. The last method, rock mining, costs a fortune and takes much time. Therefore, something has to be done in order to make salt easily & cheaply in any clime.

We, in this study, used the sponge method, plain evaporation, microwave use & with magnifying glass to extract sodium chloride out of saewater. We determined methods by economical side, product particles size, evaporation time and…

2. Experiments

2.1. First Method

A magnifying glass with 0.40 mm is used to centralize sunlight (increase the intensity of light) on bottom of the stainless steel mug or pan. After passing hours (about 4-5 h) vaporization at noon (10AM-2PM), seawater (0.7 g salt in 20cc) has been crystalized (Pan`s surface area was about 79 cm^2). It is needed to say that the cube in center of pan includes 83% silver (for the most heat transfer) and 17% cadmium (Figs.1 and 2) .

This method is extremely good for sunny countries but in other countries there is another way:

using lamps→

I put 20 cc pure seawater in small pan 9 cm under 60 watt Incandescent lamp and it took 172 minutes to crystalize completely (Fig. 3).

Figs 1 : Experimental setup

Fig. 2: The Ag- cube helps conducting heat between metals and fluid

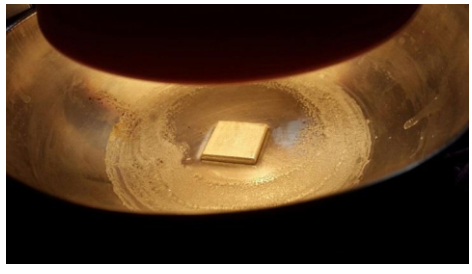

Fig. 3: After 172 minutes

2.2.Second Method

I poured seawater in a bowl with a sponge inside it.

After seconds, the sponge has been taken out and put in room temperature so it is resulted large crystals (Fig. 5). Here, different materials such as cellulose sponge, dry sponge, compressed cellulose sponge and floral foam with different porosity have been used. After using, it was washed but in big industry, it must be made very wet [5] and put in microwave for two minutes (at 1000 watt power) or in dishwasher to stay clean[6]. For extracting salt crystals in sponge, 99% ethanol was used to dissolve salt in the sponge, and as long as it was gone out, ethanol evaporated so fast (Figs. 4 , 5 and 6).

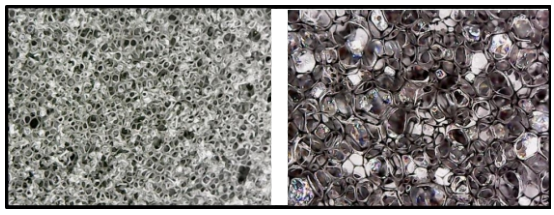

Fig.4: Salt crystals in floral foam with different grandiosity captured by lens

Fig. 5: The extracted salt from the sponge using 99% ethanol

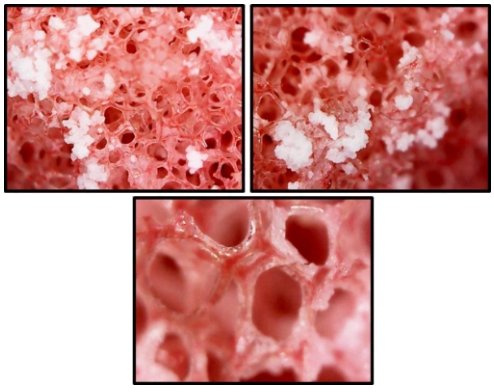

Fig.6: Salt crystals in cellulose sponge with different grandiosity captured by a lens

2.3. Third Method

This is the plain evaporation. Anywhere else in the world, everyone have access to simple equipment such as things make them able to extract salt out of seawater which will be explained.

Filter paper and cotton cloth were used to separate impurities (Fig.7). Then it was boiled and dried by sun power or surface evaporation at ambient temperature etc (Fig. 8).

Fig. 7: Separating impurities with two layers cotton cloth and Filter paper in a cone

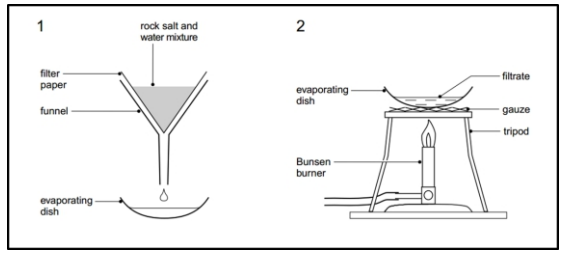

Fig. 8: Experimental Setup

2.4. Fourth Method

I put 20 cc filtered seawater solvent into microwave oven.

First time→

I put 0.7 grams salt in 20 cc water solvent, in microwave oven with 720 power for 14 seconds less than 2 minutes in which I opened the door in disorganized intervals(Fig.9).

Fig.9: Crystallite salt in 7 cm height glass mug

Second time→

I put 0.7 grams salt in 20 cc water solvent, in microwave oven with 720 power for 3 minutes and I opened the door six times in 30 seconds intervals (Fig.10).

Fig.10: Crystallite salt with 0.7 grams salt

Third time→

I put same amount of saltwater in microwave oven with 720 power for 2 minutes nonstop (Fig.11).

Fig.11: Crystallite salt with 0.7 grams salt in different power

Fourth time→

I put the same amount of seawater in microwave oven with 900 power for 2 minutes and I opened the door four times in 30 seconds intervals (Fig. 12).

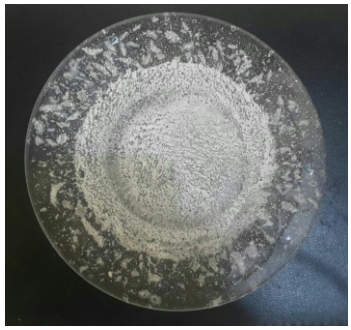

Fig.12: Crystallite salt with 0.7 grams salt in 900 power 2 min.

Fifth time→
I put same amount in, like I did, with 900 power for 1.5 seconds nonstop (Fig. 13) .

Fig.13: Crystallite salt with 0.7 grams salt in 900 power in 1.5 min.

3. Results and Discussion

Saltwater evaporation process is better to be done on cellulose pointy corner (Fig.14). Large pore-sizes in sponge causes larger salt crystal size (of about sub-millimeter) formation. Hence, they can be separated from sponge surface easier. After taking sponge out of water, must be careful not to preventing any contact between sponge and the heat sources. Any contact would be resulted in growing very small size crystals within the porosities of the sponge which cannot be extracted well.

Fig.14 : The grown salt on the pointy uneven surface of the utilized sponge

Two layers cotton cloth filter, is the best filter because it`s more accessible then filter paper and as well as it (Fig.15).

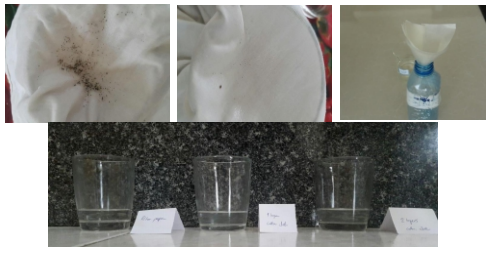

Fig.15: Comparing resulted salts from different filters

So that Seawater contains more dissolved ions than all types of freshwater[8], Producing salt at home is healthier because of iodine (I) Existence. In fourth method, with more surface, seawater is more evaporated and it can be done with huge amount of seawater. In fourth method I used green energy and it`s totally economical because most of microwaves energy use is about 900 watt. We got 0.6117 g salt out of 0.71g, and the wasted salt is about 0.0983 g which can be ignored in huge amount. Due to LPG price (0.57 U.S. Dollar per liter) [9] plain evaporation is affordable. Increasing rate of heating lead to small crystal size, while decreasing in rate of heating lead to large crystal size (Fig.16).

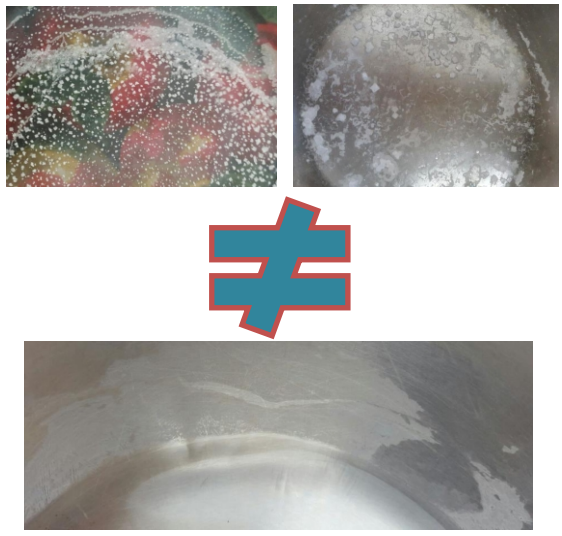

Fig. 16: Gradual, and fast evaporating

Heating process and time are two effective properties in salt crystal size. (Fig.17). According to this study, if sponge is heated immediately after being gotten out of saltwater, blank spaces in sponge would be all full causing larger salt crystals (Fig. 18). More power is needed to spend less time on evaporating saltwater in microwave oven and changes in time are mostly for interrupted processes which I opened the door in organized intervals(Fig. 19). Best sponge for extracting salt with is cellulose sponge.

Fig.17: I warmed the cellulose sponge on the left with a hair dryer for two minutes at 10 cm above it but the sponge on the right wasn't connected to any special heat sources which resulted growing large crystals.

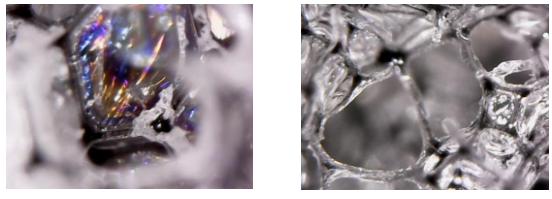

Fig.18: Salt crystals within immediately warmed cellulose sponge pros (in the left) & slow dried one (at right).

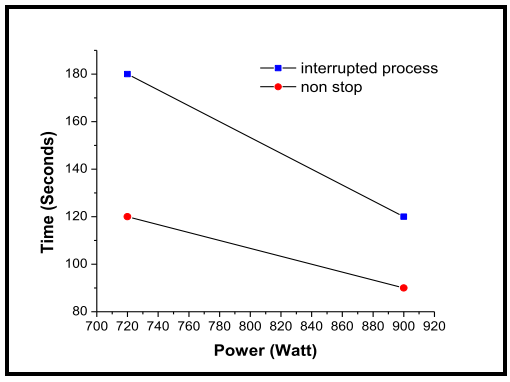

Fig. 19: The effect of microwave power on drying time

4. Conclusions

Best method is using a microwave.

Other new possible ways are: putting some amount of salt in vacuum, using Geo-thermal energy for evaporating, reverse osmosis, etc. we can make a lot of salt using Incandescent lamps and microwave. Since seawater was filtered in each experiment, all produced salt will be healthy and clean. The lowest capacity of the methods was for sponge method but it will be recovered industrial equipment.

References

[1] Institute of Medicine. Dietary reference intakes for water, potassium, sodium chloride, and sulfate. Washington, DC: National Academies Press; 2004

[2] https://seasalt.com

[3] http//www.mortonsalt.com

[4] http//www.cargil.com

[5] "Microwave 'sterilisers' warning". 24 January 2007. BBC News

[6] J. Taché etal. , Hygiene in the home kitchen: Changes in behaviour and impact of key microbiological hazard control measures". Food Control, Volume 35, Issue 1, January 2014, Pages 392–400

[7] World Ocean Atlas 2009

[8] Diagram Visual Information Ltd. Separating Salt From Rock Salt

[9] http://globalpetrolprices.com

WATER FROM THE AIR

Asal Hosseinian , Farzanegan 2 School

ARTICLE INFO

Supervisors: Mohammad Qorbani

PYNT national tournament 2017

Accepted by Ariaian Young Innovative Minds Institute , AYIMI

http://www.ayimi.org ,info@ayimi.org

ABSTRACT

Water is essential for all creatures and is one of the most important elements of our life. Rivers around the world were always respected and sacred by the communities. Having clean water plays a critical role in human civilization. One of the most important problem these days is that we don t have enough water for drinking, so we want to use the water in the air too .In this investigation, we are looking at a way to convert air moisture into drinkable water the easy way is to cool the air down to below the dew point. Byheating up and then cooling down the air inside a closed container. The water produced is distilled water, unless contaminated after/during condensation .

Keywords : *Clean Water, Condensation, Cooling, Air*

1. Introduction

As of yet, many people are not aware of water's importance and necessity in their lives. All the sources of water around the world exists naturally in different forms and locations: 1- in the air, 2- on the surface, 3- below the ground, .one of the most important problem this days it that we don t have enough water for drinking, so we want to use the water in the air too .In this investigation, we are looking at a way to convert air moisture into drinkable water the easy way is to cool the air down to below the dew point. By heating up and then cooling down the air inside a closed container. The water produced is distilled water, unless contaminated after/during condensation .

If you ask people what is the largest reserves in the world they will probably answer oil or iron or copper. Of course, which is not the correct answer since water is the world's largest reserves. In the form of surface water, under river flow, groundwater, frozen water.97% of the water on the earth is salt water and only three percent is fresh water; slightly over two thirds of this is frozen in glaciers and polar ice caps [1]. The remaining unfrozen freshwater is found mainly as groundwater, with only a small fraction present above ground or in the air.

Due to global warming and reduction in underground water supply, we need to come up with an idea to use all water reservoirs especially the water in the air. Water is present as a liquid and as a gas in the atmosphere. When water is a gas, it is called water vapor. You can't see water vapor in the air, because water molecules are very small. When water is a liquid, you can see it in the form of clouds. It can also fall from the sky as precipitation. The amount of water vapor in the air is called humidity. The amount of water vapor the air can hold depends on the temperature of the air. Warm air can hold more water vapor, while cold air cannot hold as much.

In here, we were used a method to convert air moisture into drinkable water [2]. This purpose was done by inventing a new system. The mechanism behind this novel system is: heating up and then cooling down the air inside a closed container. The water produced is distilled water, unless contaminated after/during condensation.

Water is present as a liquid and as a gas in the atmosphere. When water is a gas, it is called water vapor. You can't see water vapor in the air, because water molecules are very small. When water is a liquid, you can see it in the form of clouds. It can also fall from the sky as precipitation .The amount of water vapor in the air is called humidity. The amount of water vapor the air can hold depends on the temperature of the air. Warm air can hold more water vapor, while cold air cannot hold as much. We describe how much water vapor is in the air by using the term relative humidity. Relative humidity tells us how much water vapor is in the air, compared to how much it could hold at that temperature. It is shown as a percent. For example, a relative humidity of 50 %means the air is holding one half of the water vapor it can hold. Again, this is all dependent on the temperature. If the amount of water vapor in the air stays the same, but the temperature goes down, the relative humidity will increase. This is because the colder air cannot hold as much water vapor.

If the temperature gets cold enough, the air gets to the point that it is holding the most water vapor it can hold. The relative humidity for this temperature would be 100 percent. This is also known as the dew point temperature. Why do you think they call it this? Think of what happens on cool nights. If the temperature gets down to the dew point, some of the water vapor turns back to liquid water – this is called condensation. What do you see in the morning? That dew is just liquid water that has condensed out of the air. It is the same thing that happens when you have a cold glass of something and let it sit for a while- what happens to the outside of the glass?

With all explanation above we started with a cold cone shape steel in a warm environment such as room temperature, but there always will be the problem of not having enough high temperature to help the process. Therefore, I decided to create the hot environment and guide the air into that.

2. Experiment

For that part of the project we used a steel closed container (Fig.1) which we could warm it up, with two holes on, one for air entrance and the other one for hot air exit.

By attaching a cone on air entrance hole and using small fan we were able to force the air into the hot container and by having spiral copper wire with downward slope on the exit hole we could reduce the air temperature (by putting

temperature (by putting the copper wire in the ice water) and convert it into water drops and collect it (Fig. 2).

Fig. 1: Main Container

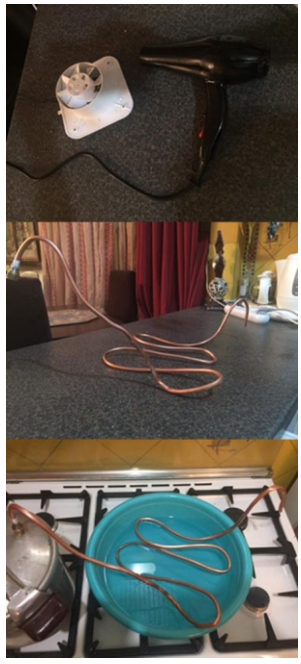

Fig.2: Small fan to make a flow of air into the system; Spiral copper wire; and the condensation container

3. Results

I tried my device and measured the amount of water that I got (Fig. 3).

We wanted to get more water so, we repeated the test by using boiling water and forcing steam into the device which gave us more water (Fig. 4).

I know my water is drinkable for using daily. Then by measuring the water's PH we made sure that the result water is drinkable.

As researches show using distilled water is more useful than natural spring waters since it is possible that spring water has more minerals that what our body needs and make some health sophistication for our body.

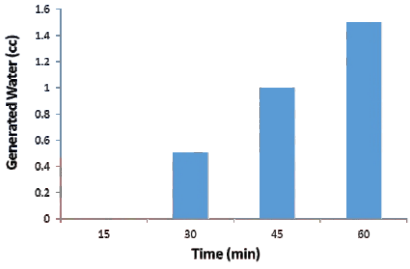

Fig. 3: Generated Water versus Time

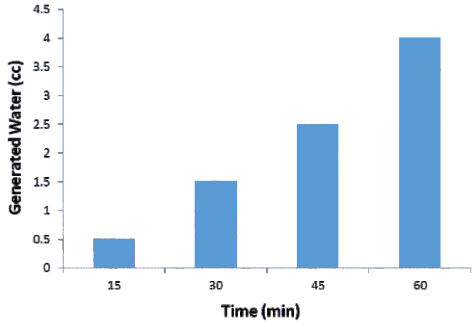

Fig. 4: Generated water by using boiling water

4. Conclusion

Water is one of the most important substances on earth. All plants and animals must have water to survive. If there was no water, there would be no life on earth. Apart from drinking it to survive, people have many other uses for water. Knowing that we experimented a way to produce distilled water from the air moisture and gave an idea to have more water.

References

[1] http://www.greenfacts.org/en/water-resources/

[2] Theresa A. McHugh, et al., Water from air: an overlooked source of moisture in arid and semiarid regions, Scientific Reports 5, 13767 (2015).

OBTAININ BIOPLASTIC WITH UPCYCLE METHOD AND INVESTIGATION OF THE EFFECT OF BIOPLASTIC COATING ON CHEESE DURING STORAGE PROCESS

[1]Serpil Korkmaz,[2] Buse Özcan. [3]Mithat Rüzgâr Özen, [4]Mariam Sayegh , 1,2,3,4 Gemlik Science High School , serpilk_35@hotmail.com

ARTICLE INFO

First Place in Izmir IISEEF 2024

Accepted by Ariaian Young Innovative Minds Institute , AYIMI

http://www.ayimi.org ,info@ayimi.org

ABSTRACT

In this study, orange peels were used to obtain pectin; biodegradable film was obtained by adding olive leaf extract obtained by supercritical CO2 extraction method to the films obtained with the addition of gelatin and glycerol as plasticizer; it was used as a coating material for basket cheese. Olive (Olea europaea) leaves were dried; extract was obtained in a supercritical CO2 extraction device at 100 ^{0} C, 300 bar pressure, 1 L/min CO2 flow rate in the presence of methanol co-solvent.

Keywords : *Supercritical CO2 Extraction, Olive Leaf Extract, Orange Pectin, Bioplastic Coating, Basket Cheese*

1. Introduction

Edible films and coatings are used to prevent food spoilage, extend shelf life and provide environmentally friendly packaging. Olive leaf (Olea europaea) is a by-product rich in bioactive policy and high economic value, but it generally remains as agricultural waste in Turkey. Supercritical systems extraction method is a modern technique for efficiently obtaining olive leaf components. Pectin is a food storage emulsifier, gelling agent and stabilizer polysaccharide obtained from waste such as orange peel and used in biofilm production.

This study aims to determine the physical and technological properties of orange pectin and gelatin added films, to obtain olive leaf extract by supercritical CO2 extraction method and to test the antimicrobial ones. In addition, the potential of these films to prevent mold formation and extend shelf life by applying them to basket cheese is evaluated. The study contributes to the development of environmentally friendly alternatives in food packaging.

It was aimed to investigate the changes in mechanical, microbiological and sensory qualities of basket cheeses coated with pectin-gelatin structured bioplastic coating material added with olive leaf extract obtained with supercritical CO2 extract and to extend the shelf life of the cheeses.

In this study, orange peels were used to obtain pectin; biodegradable film was obtained by adding olive leaf extract obtained by supercritical CO2 extraction method to the films obtained with the addition of gelatin and glycerol as plasticizer; it was used as a coating material for basket cheese. Olive (Olea europaea) leaves were dried; extract was obtained in a supercritical CO2 extraction device at 100 ^{0} C, 300 bar pressure, 1 L/min CO2 flow rate in the presence of methanol co-solvent. Olive leaf extract (OLE) was added to the film solutions at the rates of 0%, 1% and 2%. Mass and volume loss, moisture retention, water vapor permeability, thickness, tensile rupture tests, antioxidant capacity, sensory analysis, L*. a *. b *, antimicrobial analysis were performed on biofilms and cheese samples. At the beginning of the storage process,15. and at the end of the 28th day, antibiogram test was applied for Escherichia coli, Staphylococcus aereus , yeast-mold colonies. For these organisms, samples were prepared by spreading preparation method on TBX, Baird Parker and DRBC agar, respectively, and incubated at 44,25,34 ^{0} C. Yeast and Staphylococcus colonies were found on the 15th day, but mold and Escherichia coli growth was not observed. On the 28th day, starting from the control group, the number of colonies decreasing gradually towards the experimental groups was detected. Water vapor permeability of biofilms was found to be close to thickness. They were (0.0442-0.0557); (0.0554-0.0670), respectively. No significant difference was found for sensory analysis. Hardness, mass and volume loss of biofilms, decrease in a* and b* values were observed. These values are (13.98-7.59) ;(6.77-4.48); (-0.18-1.53) ;(34.94-23.52), respectively. An increase was observed in moisture content, tensile strength, percent elongation at break, adhesiveness, antioxidant capacity and L* values. These values were determined as (7.48-11.12) ;(0.499-0.561) ;(0.390-0.393) ;(0.266-0.323) ;(0.17-0.74) and (66.4 80.59), respectively. In our study, edible films were prepared using gelatin-pectin biopolymer and olive leaf extract; the physical, mechanical and antimicrobial properties of the films were characterized. It was shown that the prepared films could be an alternative to currently used food packaging.

2. Materials and Methods

Gemlik olive leaves exposed as a result of pruning in Bursa-Gemlik were collected .

The peels used in the study were obtained from fresh orange fruits obtained from the local market. Orange (Citrus sinensis) peels (albedo part) were cut into 1 cm2 square pieces with a knife ; dried in an oven at 50°C for 48 hours and then ground in a grinder. Glycerol (99.5%) was used to eliminate the brittleness of the films and increase their elasticity. Methanol, which we used as a co-solvent in supercritical CO2 extraction, citric acid monohydrate and ethanol, which we used in pectin production, were purchased from Merck Chemicals Co. (Darmstadt, Germany). Gelatin used in biofilm production was supplied from a local herbalist; basket cheese used for application to the films was supplied from a local producer company.

2.1. Pectin Production

peel powder was treated with pH=2 citric acid solution at 80°C for 60 minutes. The mixture was precipitated with ethanol, filtered and dried. Pectin samples were dried at 50°C and stored at +4°C.

2.2. Supercritical-CO2 (SC-CO2) Extraction

From olive leaves with SC-CO 2. 100 g of leaves were extracted at 300 bar pressure and 100°C temperature. Methanol was used as a co-solvent during extraction. Extracts were stored in dark and cold conditions until analyzed.

2.3. Edible Biofilm Film Preparation

Biofilms were prepared using pectin (2%), gelatin (2%), and glycerol (7%). Olive leaf extracts obtained by supercritical extraction were added to the film at 0%, 1%, and 2% rates. The films dried in petri dishes were kept in a desiccator for 48 hours.

2.4. Coating Cheese with Film Solution

The sterilized cheese samples were coated with (0%, 1%, and 2% olive leaf extract added films). The samples were stored at +4°C. After the coating process applied by the immersion method, the cheeses were dried and sterilized.

3. Analysis

3.1. Film Thickness Measurement and Mechanical Property Analysis

Film thicknesses varied between 1.440-1.480 mm. As the amount of olive leaf extract increased, hardness decreased and adhesiveness increased.

3.2. Determination of Total Moisture Content

The moisture content of the films varied between 7.48% and 11.12%. The highest moisture content was measured in films containing 1% olive leaf extract.

3.3. Determination of the Effect of Films on Mass and Volume Change Rates of Cheese Samples

Mass and volume changes of coated cheeses were calculated. Films with 1% and 2% olive leaf added retained more moisture.

Volumetric Change (%) = [(V initial – V final)/ V initial] x 100 Equality(1)

Mass Change (%) = [(m initial – m final)/ m initial] x 100 Equality (2)

3.4. Water Vapor Permeability (WV)

Water vapor permeability of biofilm samples was determined according to ASTM management. Water vapor permeability rate revealed the properties of the films.

$$\frac{dW}{d\text{ø}} = \frac{K\,A(p1-p2)}{X} = \frac{K\,A\,\Delta p}{X} \qquad \text{Eşitlik (3)}$$

Here dW/dø; represents the rate of water gained or lost in a day, A; area, p1 and p2; represents the vapor pressure of water between the two sides of the film, and (Δp); p1–p2. The K/X ratio is also expressed as the water vapor permeability rate of the film (Akşehir, K., 2013) .

3.5. L*. a *. b* Color Analysis

Color determination was made by using flash beams sent from the device to the cheese pieces, the measurements were reflected on the screen of the device, and then statistical evaluation was made.

4. Antioxidant Capacity Determination (DPPH Method)

Antioxidant capacity determination experiments were carried out at Tubitak Butal Laboratory under the supervision of laboratory personnel.

4.1. Microbiological Analysis

Preparation of Samples for Analysis

Cheese samples were prepared in sterile stomacher bags, 90 mL Buffer Pepton Water was added to 10 g of cheese and turned into a solution. Samples were mixed in the Stomacher device for 1 minute, diluted to 10^{-1} level and made ready for cultivation. At the beginning of the storage process, at the end of the 15th and 28th days , antibiogram tests were applied for Escherichia coli, Staphylococcus aereus , yeast-mold colonies. Samples were prepared for these organisms by the smear preparation method on TBX, Baird Parker and DRBC agar, respectively, and incubated at 44, 25, 34 0 C.

4.2. Sensory Analysis

The coated cheese samples were evaluated with a hedonic scale for appearance, taste, odor and overall liking. The tests were performed by the panelists on days 0, 15 and 28. The samples were evaluated with a hedonic scale of 1-9 for appearance, color, texture, taste and odor and overall liking criteria: 1-3 (unacceptable), 4-5 (acceptable), 6-7 (good), 8-9 (very good).

4.3. Statistical Analysis

Statistical analysis of the data obtained as a result of the analyses was carried out using the SPSS package program (version 28.0), Kruskal Wallis analysis was performed to determine the differences and the Mann Whitney U test was applied for statistically significant differences.

5. Results

Measurement of Thickness and Mechanical Properties of Films

Prepared olive leaf extract containing pectin-gelatin added films The arithmetic average of the hardness and adhesiveness, tensile-rupture analyzes performed at 5 different points on the TA. XT Plus C brand (10N (1kg) Capacity / 0.001N (0.1g) Sensitivity) texture analyzer was calculated and shown in Table (1).

Table (1): Hardness and Adhesion Analysis Results of Films

Product	Hardness (N)	Stickiness (Ns)
K	8.071 ± 0.008^a	0.266 ± 0.008^a
0	6.338 ± 0.008^a	0.282 ± 0.008^a
1	3.264 ± 0.008^a	0.315 ± 0.008^a
2	3.032 ± 0.008^a	0.323 ± 0.008^a

(K: uncoated sample, 0: coated with only pectin and gelatin, 1: 1% OLE added, 2: 2% OLE added cheese) It is seen in Table 1 that as the amount of olive leaf extract of the biodegradable films increases, their hardness decreases and their adhesiveness value increases. When the values are examined, it can be said that the biofilm with the softest and most adhesive structure is the sample with 2% olive leaf added.

5.1. Measuring the Thickness of Films

The thickness of edible film samples was measured with a digital electronic micrometer and the average of 10

random measurements was taken. The thickness of the gelatin-pectin structured films containing olive leaf extract varied between 1.440 and 1.480 mm. The thinnest film contained 1% olive leaf extract, while the thickest film had only gelatin-pectin structure.

5.2. Mechanical Properties of Films

Tensile Strength and Elongation Percentage: While the tensile strength of the films represents the resistance against external forces, the elongation percentage expresses the geometric change. The highest elongation percentage at break was observed in the films containing 1% olive leaf extract (34.83%). The highest tensile strength was also determined in the biofilm containing 1% olive leaf extract (0.561).

Table (2)

No	Renk	Tarih	Max. Kuvvet N.	Gerilme MPa	Max.Kuvvet Uzaması mm.	Kopmada Yüzde Uzaması	Numune mm.
1		25.12.2023 10.32	7.2	0.499	31.027	0.390	1.450
2		25.12.2023 10.48	8.1	0.561	34.830	0.393	1.440
3		25.12.2023 10.51	8.04	0.542	32.834	0.393	1.480
		Ortalama	7.78	0.534	32.897	0.392	1.456
		St. sapma	0.41	0.023	2.069	0.0014	0.017
		En büyük	8.1	0.561	34.830	0.393	1.480
		En küçük	7.2	0.197	31.027	0.390	1.440

1-%2 ZYE katkılı biyofilm, 2-%1 ZYE katkılı biyofilm,3- saf pektin-jelatin katkılı film

Table (3)

No	Renk	Tarih	Max. Çekme Dayanımı (MPa)	Max. Çekme Dayanımındaki Uzama (%)	Elastik modül (MPa)
1		25.12.2023	0,499	77,58	0,612
2		25.12.2023	0,561	87,13	0,600
3		25.12.2023	0,540	84,43	0,602
		Ortalama	0.866	83.71	0.604
		St.sapma	0.133	0.261	0.0174
		En büyük	0,561	87,13	0,612
		En küçük	0,499	77,58	0,600

1-%2 ZYE katkılı biyofilm , 2-%1 ZYE katkılı biyofilm ,3- saf pektin-jelatin katkılı film

6. Humidity Rate

The percentage moisture content of the film samples was calculated as the weight loss that occurred as a result of drying approximately 5 g of the film sample at 105ºC until it reached constant weight (AOAC, 2000).

Table (4): Total moisture content of control and experimental group films (%)

Sample	Total Moisture Content (%)
K	7.48± $^{0.071d}$
0	9.76±0.284 ^{abc}
1	$^{11.12}$ ± 0.981a
2	10.54±0.336 ^{ab}

(K: uncoated sample, 0: coated with only pectin and gelatin, 1: 1% OLE added, 2: 2% OLE added cheese)

The total moisture content of the films belonging to different film samples was observed to vary between 7.48% and 11.12%. While the lowest moisture content was determined in the control (uncoated) cheese group, the highest moisture content was determined in films containing 1% olive leaf extract.

7. Determination of the Effect of Films on Mass and Volume Change Rates of Cheese Samples

with an initial mass of ~ 10 g and a volume of ~ 8 cm3, covered with K,0,1,2 coded films and kept at +4 o C for 30 days were taken out of the refrigerator during the measurement and their mass and volume were measured; the measurements were repeated 5 times and their averages were taken. Percentage mass (moisture) and volume loss were calculated using Equation 1 and Equation 2 (Table 5).

Table (5): Volume and Mass Change Percentage of Cheese Samples Coated with K,0,1,2 Films

Product	V_{end} (cm^3)	m_{last} (g)	Volume Loss (%)	Mass Loss (%)
K	7.46±0.006 ^{B}	8.61±0.010 ^{Bar}	6.77±0.014 ^{Aa}	13.98±0.011
0	7.61±0.007 ^{Bb}	8.904±0.005 ^{Aa}	4.82±0.006 ^{Ab}	10.96±0.007 ^{ABab}
1	7.64±0.007 ^{ABab}	9.211±0.008 ^{Cb}	4.48±0.014 ^{Bb}	7.59±0.007 ^{Aa}
2	7.64±0.005 ^{Ab}	9.748±0.012 ^{Bb}	4.48±0.006 ^{Ab}	7.62±0.019 ^{Ab}

(K: uncoated sample, 0: coated with only pectin and gelatin, 1: 1% OLE added, 2: coated cheese with 2% OLE added)

The volume loss rates of the samples were found to be between 6.77 and 4.48%; mass loss was found to be between 13.98 and 7.59. The best results in terms of both values were found in samples with 1% olive leaf extract; the highest loss was found in samples from the control group.

8. Water Vapor Permeability (WVP)

Water vapor permeability not only affects the freshness of the product but also has an effect on microbiological development (Kopacic et al., 2018). Water vapor permeability (WVP) values of the film samples are given in Table (6).

Table (6) : Water Vapor Permeability (WVP) Values of Film Samples (g mm/m2 h kPa)

Product	1st attempt	2nd attempt	3rd attempt
0	0.0557 ± 0.0023 ^{b}	0.0564 ± 0.0034 ^{b}	0.0555 ± 0.0032 ^{b}
1	0.0496 ± 0.0022^{c}	0.0442 ± 0.0033^{c}	0.0472 ± 0.0033^{c}
2	0.0538 ± 0.0036 ^{b}	0.0522 ± 0.0036 ^{b}	0.0529 ± 0.0036 ^{b}

(0: film sample coated with only pectin and gelatin, 1: 1% OLE doped, 2: 2% OLE doped)

In our study, the WVP values of gelatin-pectin films with olive leaf extract added varied between 0.0442-0.0598 g.mm/m²h.kPa. The lowest WVP was determined in films containing 1% OLE and the highest in pure pectin-gelatin films. (p >0.05). The WVP values in our study were lower than these samples and it was thought that the olive leaf extract had a reducing effect on moisture loss.

9. Analysis of Optical Properties of Films

The L*, a* and b* values of the film-coated basket cheese samples were measured three times with a light beam sent in the form of a flash from a cube-shaped cheese piece placed in the special chamber of the device. The arithmetic average of the values obtained was taken and the color determinations of the films were made. The first reading values are shown in Appendix-3; their evaluations are shown in Table (7).

Table (7) : L*, a* and b* values of film samples

Product	L *	a *	b *	C*	h *
K	66.4±2.20 ^{A}	1.53±1.50 ^{A}	34.94 ±1.22 ^{Aa}	34.97±1.48 ^{A}	87.496±1.62 ^{Aa}
0	77.05 ±153 ^{Aa}	0.87 ±0.50 ^{Aa}	33.98 ±1.62 ^{Aa}	33.986±1.41 ^{Aa}	88.53±.38 ^{Aa}
1	70.58 ±3.36 ^{Aa}	1.05 ±1.12 ^{Aa}	34.03±1.24 ^{A}	34.02±1.10 ^{A}	88.22±1.36 ^{A}
2	80.59 ±2.46 ^{Aa}	-0.18 ±0.10 ^{Aa}	23.52±1.38 ^{A}	23.52±1.10 ^{Aa}	90.43±2.48 ^{A}

(K: uncoated sample, 0: coated with only pectin and gelatin, 1: 1% OLE added, 2: 2% OLE added cheese)

According to the data, the olive extract ratio L* (lightness-darkness), a* (red-green), b* (yellow-blue), C* (saturation) and h* (color tone difference) values

increased. As a result of statistical analysis, it was tested that the extract data had a significant effect on these properties.

10. Antioxidant Capacity

Antioxidant capacity in film samples was determined by the % DPPH method. The % DPPH values of the film samples are given in Table (8).

Table (8): Antioxidant capacity values of film samples

Sample	Experiment name	Unit	Test Method	Experimental Result Mean
Pure pectin-gelatin	Antioxidant Capacity (in Trolox equivalents)	µmol/g sample	With DPPH	0.17 ± 0.01
Added 1% olive leaf extract	Antioxidant Capacity (in Trolox equivalents)	µmol/g sample	With DPPH	0.37 ± 0.09
2% olive leaf added	Antioxidant Capacity (in Trolox equivalents)	µmol/g sample	With DPPH	0.74 ± 0.06

The antioxidant capacity of the control sample, which was 22.39%, increased significantly ($p<0.05$) with the addition of olive leaf extract (OLE) to the film solution, and the film sample containing 2% OLE showed the highest value at 74%. These results are consistent with the study of Liu et al. (2021), revealing that OLE is effective in increasing the antioxidant capacity.

11. Microbiological Analysis

The change in the amount of microorganisms at the end of the 28-day storage period is presented in Table (9).

Table (9): Change in microorganism loads of cheese samples during storage (log cfu/g)

Microorganism	Sample	Day 0	Day 15	Day 28
Escherichia coli	K	0	1.78 ^{aA}	3.50 ^{bcC}
	0	0	0.22 ^{aA}	2.05 ^{bcC}
	1	0	0	1.70 ^{Aa}
	2	0	0	1.50 ^{abA}
Coagulated Staphylococcus aereus	K	0	4.45 ^{aA}	5.67cc
	0	0	3.05 ^{aA}	5.15cc
	1	0	2.40 ^{bB}	3.15 ^{abB}
	2	0	1.08 ^{bB}	3.03 ^{aB}
Mold (*Aspergillus flavus)* colonies	K	0	3.32 ^{aA}	5.83 ^{bB}
	0	0	2.12 ^{aA}	5.85 ^{bB}
	1	0	0	1.34 ^{aB}
	2	0	0	1.28 ^{aB}
Yeast colonies	K	0	3.80 ^{aA}	5.40 ^{cc}
	0	0	3.68 ^{aA}	5.05 ^{bB}
	1	0	1.50 ^{aB}	3.85 ^{bA}
	2	0	1.40 ^{bbc}	3.02 ^{bB}

(K: uncoated sample, 0: coated with only pectin and gelatin, 1: 1% OLE added, 2: 2% OLE added cheese)

While no microorganisms were detected in samples exposed to UV rays and sterilized, E. coli , mold, S. aureus and yeast growth was observed. In samples with 1% and 2% OLE, microbial growth decreased significantly, especially the 2% OLE added coating gave the most effective results ($P<0.05$). These results show that olive leaf extract is effective in microbial inhibition.

12. Sensory Analysis

Pectin-gelatin structure with olive leaf extract additive The sensory analysis results of basket cheese samples stored covered with biofilm are shown in Table (10).

During storage, appearance, color, taste, odor and general appreciation scores tended to decrease in all samples ($P<0.05$). However, OLE-added samples received higher scores than the control group. At the end of the 28th day, the most appreciated sample was cheese with 1% OLE, while the control sample had the lowest values. OLE additive affected the quality positively, especially in terms of taste, odor and structure ($P<0.05$).

Table (10): Sensory analysis results of Sepet cheeses

Criterion	Sample	Day 0	Day 15	Day 28
Appearance	301	7.75 ^{aA}	6.46 ^{aB}	5.15 ^{bcC}
	302	7.71 ^{aB}	6.75 ^{aB}	5.50 ^{bcC}
	303	6.90 ^{bA}	6.80 ^{aA}	6.70 ^{Aa}
	304	6.85 ^{bA}	6.55 ^{bA}	6.50 ^{abA}
Colour	301	7.89 ^{aA}	7.08 ^{bB}	6.05cc
	302	7.90 ^{aA}	7.15 ^{bB}	6.45cc
	303	7.25b ^{EU}	7.40 ^{aA}	7.10 ^{abB}
	304	7.35 ^{bB}	7.55 ^{aA}	7.25 ^{aB}
Structure	301	7.64 ^{aA}	7.75 ^{aA}	5.83 ^{bB}
	302	7.65 ^{aA}	7.75 ^{aA}	5.85 ^{bB}
	303	7.70 ^{aA}	7.75 ^{aA}	6.40 ^{aB}
	304	7.75 ^{aA}	7.95 ^{aA}	6.55 ^{aB}
Taste and Smell	301	7.75 ^{aB}	7.00 ^{bbc}	6.55cc
	302	7.65 ^{bB}	7.85 ^{aB}	7.55 ^{bB}
	303	8.15 ^{abA}	8.40 ^{aA}	7.80 ^{bA}
	304	7.85 ^{eu}	8.05 ^{aA}	7.40 ^{bB}
General Like	301	7.75 ^{aA}	7.20 ^{bab}	5.80 ^{cc}
	302	7.30 $^{a.b.}$	7.30 $^{a.m.}$	6.55 ^{bA}
	303	7.30 $^{a.b.}$	7.35 ^{aA}	6.80 ^{bA}
	304	7.20 ^{aAB}	7.25 ^{aAB}	6.75 ^{bAB}

(301-control, 302 pure gelatin-pectin, 303 1% OLE added, 304 2% OLE added biofilm coated cheese sample)

13. Conclusion and Discussion

In recent years, economical and antimicrobial biofilms have been developed as an alternative to synthetic polymers in food packaging. The usability of these gelatin-pectin based biopolymers as packaging has been tested. In the literature, there is no study on films made biocomposite with glycerol and the use of olive leaf extract with the supercritical CO 2 method. The use of orange peel and olive leaf has supported the environmentally friendly aspect of the product. The mechanical and physical properties of the films were examined, and it was found that olive leaf extract did not create a significant difference in the tensile strength, elongation percentage and elastic modulus of tension, but there were more homogeneous structure temperatures. In antimicrobial tests, it was determined that films containing olive leaf extract were effective against Staphylococcus aureus and yeasts, and Escherichia coli and mold colonies were not detected in 15-day storage. These films are appropriately selected for packaging basket cheese, which shows higher antimicrobial activity compared to controls. In addition, the phenolic substance and flavonoid content is increased, thus protecting human health and the environment.

References

[1] Akarca, G., Çağlar, A., & Tomar, O. (2016). The effects of spicing on quality of mozzarella cheese. Mljekarstvo, 66(2), 112-121. http://doi.org/10.15567/mljekarstvo.2016.0203 .

[2] Bátori, V., Jabbari, M., Åkesson, D., Lennartsson, PR, Taherzadeh, MJ, Zamani, A. 2017. Production of pectin -cellulose biofilms: a new approach for citrus waste recycling. International Journal of Polymer Science, 2017.

[3] Debeaufort, F., Martin -Polo, M. and Voilley, A. (1993). Polarity Homogeneity and Structure Affect Water Vapor Permeability of Model Edible Films. Journal of Food Science 58, 426-434.

[4] Guilbert, S. 1986. Technology and application of edible protective films, p. 371. In M. Mathlouthi (ed.), Packaging and preservation theory and practice. Applied Science, Elsevier, New York.

[5] Guında, À, 2006, Use of solid residue from the olive industry, Grasas Aceites , 57 (1), 107-115.

[6] Jridi, M., Abdelhedi, O., Salem, A., Kechaou, H., Nasri, M. & Menchari, Y. (2020). Physicochemical, antioxidant

and antibacterial properties of fish gelatin based edible films enriched with orange peel pectin: Wrapping application. Food Hydrocolloids, https://doi.org/10.1016/j.foodhyd.2020.105688 1

[7] Kopacic, S., Walzl, A., Zankel, A., Leitner, E. & Bauer, W. (2018). Alginate and Chitosan as a Functional Barrier for Paper-Based Packaging Materials. Coatings, 8(7), 235. https://doi.org/10.3390/coatings8070235

[8] Krochta J.M. and Mulder-Johston C. (1997). Edible and Biodegradable Polymer Films Challenges and Opportunities. Food Technology, 51 (2), 61-74.

[9] Mylonakı, S., Kıassos, E., Makrıs, DP, Kefalas, P., 2008, Optimization of the extraction of olive (Olea europaea) leaf phenolics using water/ethanol-based solvent systems and response surface methodology, Analytical and Bioanalytical Chemistry, 392 (5), 977-985.

[10] Sarıcaoğlu, FT (2019). Mechanical and Barrier Properties of Edible Films Produced from Hazelnut Proteins Applied with High Pressure Homogenization Process. Food , 45 (1), 115-124.

INVESTIGATION OF THERAPEUTIC EFFECTS OF DIFFERENT CEREAL PRODUCTS ON ALZHEIMER'S DISEASE CAUSED BY AICI3

Asım Fatih SOYDAN , cananbilsemizmir@gmail.com

ARTICLE INFO

First Place in Izmir IISEEF 2024

Advısor: Canan CIĞAL

Accepted by Ariaian Young Innovative Minds Institute , AYIMI

http://www.ayimi.org ,info@ayimi.org

ABSTRACT

Alzheimer's disease is a progressive neurodegenerative disease that is considered the most common cause of dementia in elderly individuals and slowly causes loss of cognitive functions. Today, it is estimated that there are approximately 40 million Alzheimer's patients worldwide, and this number is expected to reach 115.4 million by 2050.This study aims to investigate the protective and therapeutic effects of different cereal products, which have an important place in our nutritional habits, on Alzheimer's disease caused by aluminum chloride (AlCl3). The study aims to evaluate whether cereals play a potential role in the prevention and treatment of Alzheimer's disease.

Keywords : *Alzheimer's, Cereals, AlCl3, Eisenia fetida, Acetylcholine Esterasebasket Cheese*

1. Introduction

Despite the advances in medical and health sciences today, complete success has not been achieved in the treatment of Alzheimer's disease. For this reason, preventive approaches for Alzheimer's disease have become the focus of attention.In order to protect ourselves from Alzheimer's disease, where oxidative damage increases as a result of the aging process, our current diet needs to be changed and healthy nutrition models should be implemented. (Canbolat et al, 2016)The current study is the first comparative analysis report in the E. fetidae worm model to examine the effect of eight different varieties of cereal on Alzheimer's disease caused by aluminum chloride. The two most important physical findings in the brain cells of people affected by Alzheimer's disease are neuritic plaques and neurofibrillary tangles. Pathophysiologically, Alzheimer's disease is characterized by the accumulation of hyperphosphorylated tau and beta-amyloid (Aβ) plaques in the central nervous system. (Hawkins et al, 2019). While there is some plaque in the brains of older people, excessive plaque formation is seen in the brains of Alzheimer's patients.

There is a protein called beta amyloid in the middle of these plaques. Neurofibrillary tangles are twisted remnants of a protein called "tau" that is found inside brain cells and is necessary to maintain proper cell structure and cell activity. (Campbell, 2004) The underlying mechanism of synapse loss and subsequent neuronal death in neurodegenerative diseases such as Alzheimer's is apoptosis that occurs locally in synaptic compartments. (Nonaka et al, 2019) Another important feature associated with the development of Alzheimer's disease is the decrease in acetylcholine (ACh) levels in the brain. Acetylcholine has now been revealed to have an important place in the pathogenesis of Alzheimer's and Parkinson's diseases. After acetylcholine is released into the synaptic space, it is broken down by being converted to choline and acetate with the help of the acetylcholinesterase enzyme. (Kent, 2015) .

Alzheimer's disease is a progressive neurodegenerative disease that is considered the most common cause of dementia in elderly individuals and slowly causes loss of cognitive functions. Today, it is estimated that there are approximately 40 million Alzheimer's patients worldwide, and this number is expected to reach 115.4 million by 2050.This study aims to investigate the protective and therapeutic effects of different cereal products, which have an important place in our nutritional habits, on Alzheimer's disease caused by aluminum chloride (AlCl3). The study aims to evaluate whether cereals play a potential role in the prevention and treatment of Alzheimer's disease. The California earthworm (Eisenia Fetida) model was used in the study, and diet groups were formed containing eight different types of cereals with twenty earthworms in each group. 600 mg kg-1 AlCl3 was administered to the control group and diet groups containing different cereal products by suppressing oxidative stress and neuroinflammation, and the effects of aluminum intake on survival rates in the control and diet groups were investigated. Behavioral changes in learning and memory performance of animals after neurodegeneration were analyzed using the Seymour apparatus and the duplo base plate. In our study, a significant decrease in AChE activation in the nervous system of animals administered 100 g/kg buckwheat was observed compared to worms in other diet groups, and it was determined that it was the most effective cereal type in AlCl3-induced Alzheimer's disease.

1.1. Aluminum Toxicity and Alzheimer's Disease

Genetic and environmental factors are effective in the etiology of Alzheimer's disease. (Canbolat et al, 2016) It is known that aluminum is an important cross-linking agent that immobilizes reactive molecules in brain cells. In addition, it affects free radical pathology in neurons; It causes neurofibrillary tangles. These changes are seen in brain autopsies of Alzheimer's patients. Aluminum is a strong inhibitor of choline and dopamine production. These are important mediators in nerve impulse transmission, nerve impulse transmission to muscles and various glands. As a result of this effect, Al ions in the brain affect short-term memory and thinking. (Akman et al, 2011)

1.2. Proper Grain Consumption and Alzheimer's Disease

Cereal products are the basic food source for the world population (McKevith, 2004). Cereals and cereal products are the first in food consumption throughout Turkey. On average, 44% of daily energy is provided by bread alone, and 53% by bread and other cereal products. (Şanlıer, 2013) Cereals and cereal products are an important energy

source with the macro and micro nutrients they contain.

2. Methodology

In the study, the california earthworm (Eisenia fetida) model was used, and diet groups containing eight different cereal types were created, in which there were 20 earthworms weighing 0.5 grams with clitelium in each group. Plastic containers are filled with 1000 g of soil and 100 g of different grain products (Fig. 1).

Fig. 1: The study utilized E. fetidae worms, various types of flour

3. Experimental Design

Table 1: Experimental design including control and experimental groups

Group I: Negative control group. Normal healthy worms were fed with compost soil. No AlCl3 was administered.	Group II: Positive control group. Worms were fed with compost soil induced with AlCl3 at 600 mg/kg.
Group III: White flour + AlCl3 (600 mg/kg)	Group IV: Buckwheat flour + AlCl3 (600 mg/kg)
Group V: Corn flour + AlCl3 (600 mg/kg)	Group VI: Rye flour + AlCl3 (600 mg/kg)
Group VII: Oat flour + AlCl3 (600 mg/kg)	Group VIII: Barley flour + AlCl3 (600 mg/kg)
Group IX: Rice flour + AlCl3 (600 mg/kg)	Group X: Wheat germ + AlCl3 (600 mg/kg)

3.1. Preparation of Experimental Apparatus

After aluminum chloride induction, the locomotor behavior of the earthworms was analyzed by Seymour's (1969) method. The locomotor activity of the worms was evaluated in a mica apparatus measuring (L x W x H; 16.5 x 7.3 x 7.9 cm) (Subaraja, et al., 2019). The bottom and sides of the apparatus were covered with millimeter paper scaled with 0.1 mm. All experiments were carried out in a dark room with light on the experimental apparatus. The locomotor activity of the worms in the control group and different diet groups was determined by counting the total number of lines crossed by the earthworms in a 60-second period. The movement was expressed in centimeters as the total number of lines crossed by the anterior end of the worm ("head"). The experiments were carried out on a total of 10 worms for each group. The arithmetic mean and standard deviation values were calculated for each experimental group. The rating was calculated as the total distance traveled in cm.

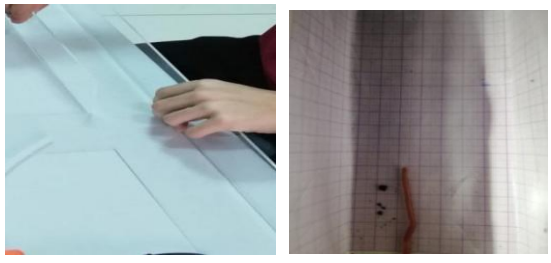

Fig. 2: Behavioral test apparatus designed for the measurement of locomotor activity

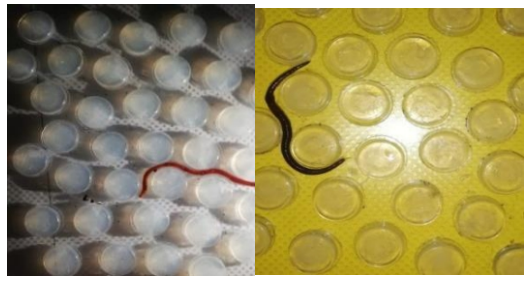

Fig. 3: Duplo base plate used in experiments that require the worms to come into contact with stoppers to advance

As a behavioral apparatus, an artificial Duplo base plate arranged in a half-moon shape was created to create a barrier for the worms. 36 pieces of 18 mm adhesive-based transparent sound stoppers were used to create the Duplo base plate. Care was taken not to create linear paths in the arrangement of the stoppers. This provided an environment where the thigmotaxic worm could feel things touching its body as if it were in the soil and the observer could still see the worm. (Walton, 1927) A stopper located on the top row of the Duplo plate was accepted as the starting point. The time spent by the experimental worms from the starting point to the exit point from the Duplo board and the total time spent on the plate were noted in seconds (Wilson et al., 2024).

3.2. Determination of Survival Rates

The number of live worms was counted on the 10th day of administration in Eisenia fetida individuals chronically exposed to 600 mg/kg-1 aluminum contraction. In the control group and the diet groups containing different cereal products, the effects of aluminum intake on survival rates in the control and diet groups were examined.

3.3. Acetylcholine Esterase Activity Test

On the 10th day of AlCl3 application, 10 clithelium earthworm samples were collected from each experimental group, weighing an average of 0.5 g, and were suitable for statistical analysis. The worms were then rinsed thoroughly with distilled water and stored at -20 °C until the homogenization process. Before the earthworms were homogenized, the samples were left on ice to thaw. After weighing the samples, a volume of cooled homogenization buffer (w/v) 4 times their weight was added to them. They were homogenized separately in 0.05 M potassium phosphate buffer (1:4 ratios, pH 7.4) in the cooled state. Each homogenate was centrifuged at 10,000 rpm in a refrigerated centrifuge for 15 minutes. The supernatant was collected and stored in a deep freezer (-20°C) until further biochemical analyses (Acharya et al, 2020) .

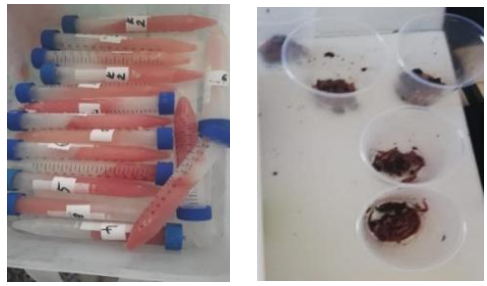

Fig. 4: Worm samples prepared for biochemical analysis before and after centrifugation

3.4. Measurement of Acetylcholine Esterase Activity

In the acetylcholine esterase (AChE) activity study; 0.1 M phosphate buffer (PBS, pH 8.0), 0.01 M 5 5'-dityiobis(2-nitrobenzoic acid) (DTNB), 0.1 U/mL AChE and 3 mM acetylthiocholine iodide (ATCI) were used. AChE activity in the supernatants obtained by centrifugation of worm homogenates was examined spectrophotometrically in a multimode microplate reader (CLARIOstar plus-BMG Labtech). 25 µL of 0.01 M DTNB, 30 µL of supernatant and 25 µL of 0.1 U/mL acetylcholine esterase enzyme were added to 150 µL of 0.1 M PBS in the microplate and incubated for 15 minutes at room temperature. At the end of the period, 25 µL of 3 mM ATCI was added and absorbances were measured at 30-second intervals for 10 minutes at a wavelength of 412 nm. AChE activity is given as nM ATCI/min. The results obtained are presented in Table (1). Measurements were made 3 times for each sample and the results are given as mean ± standard error (Albayrak et al, 2022).

4. Statistical Analysis

One-Way ANOVA analysis and LSD post-hoc test were used in the Windows SPSS 13.0 program to evaluate the results. P<0.05 was accepted as the range for determining the statistical difference.

5. Results

5.1. Survival Rates of E.fetidae Individuals in the Control and Experimental Groups Fed with Different Cereal Diets in the Presence of Aluminum Chloride

All worms survived in the negative control group not exposed to aluminum toxicity and in the buckwheat diet groups exposed to aluminum toxicity, and the survival rate was calculated as 100%. The lowest survival rates were observed in diets containing wheat germ and rice flour (70% and 80%), respectively.

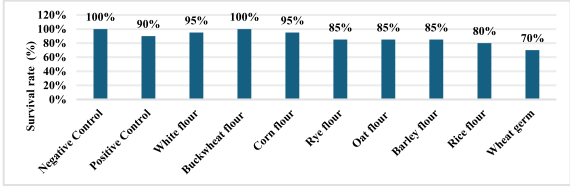

Fig. 5: Survival rates of aluminum chloride in E.fetidae individuals in experimental groups fed control and different grain diets

5.2.Measurement of Locomotor Activity

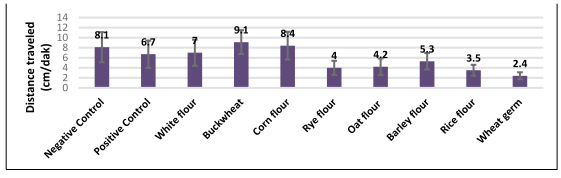

Fig. 6: Locomotor activity of worms in the control group and different diet groups (cm/min)

Table 2: Shows locomotor activity for each group (Mean ± Standard Error)

Group : Distance traveled (cm/min) = (Average ± Standard Error)				
Negative control	Positive control	White flour	Buckwheat flour	Corn flour
8,1 ±2,96	6,7 ±2,833	7 ±2,55	9,1 ±2,482	8,4 ±2,724
Rye flour	Oat flour	Barley flour	Rice flour	Wheat germ
4 ±1,316	4,2 ±1,729	5,3 ± 1,639	3,5 ±1,066	2,4 ±0,707

Depending on the study area, data representation was made with a confidence level of 99.9%. The results are presented as the mean ± SD of ten separate experiments for each group.

5.3: Duplo base plate, Coordination, Escape and Evasion Learning

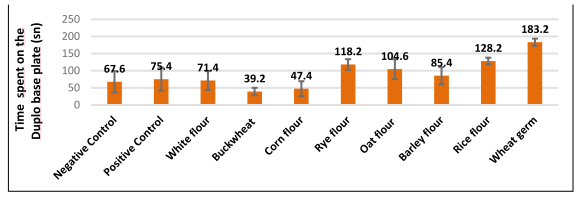

Fig. 7: Time spent on the duplo base plate of worms in the control group and different diet groups (seconds)

Table 3: Time spent by the worms in the control and experimental group on the duplo base plate (sec)

Time spent on Duplo baseplate (sec) = (Average ± Standard Error)				
Negative control	Pozitif control	White flour	Buckwheat flour	Corn flour
67,6 ±32,27	75,4 ±33,66	71,4 ±31,496	39,2 ±9,463	47,4 ±21,868
Rye flour	Oat flour	Barley flour	Rice flour	Wheat Germ
118,2 ±15,574	104,6 ±29,124	85,4 ±25,207	128,2 ±9,887	183,2 ±10,40

5.4. Effect of Different Cereal Diets on AChE "Acetylcholinesterase" Activity in Worms Exposed to AlCl3

As a result of the 10-day study, acetylcholine esterase activation (AChE) activity levels were observed in the lowest grechka (buckwheat) and corn flour at 1.11 ± 0.04 (nM ATCI/min) and 1.27 ± 0.03 (nM ATCI/min), respectively, while the highest values were 4.19 ± 0.10 (nM ATCI/min) and 2.85 ± 0.06 (nM ATCI/min) in germ and rice flour, respectively.In our study, a remarkable decrease in AChE activation in the nervous system was observed in the animals treated with 100 g/kg of grechka (buckwheat) compared to the worms in other diet groups.

Table 4: AChE activities of control and experimental groups

	Groups	AChE (nM ATCI/dk)	Significant Differences Between Groups
1	Negative Control (Fruit and vegetable compost waste)	1,56 ± 0,01	*4, 5, 6, 7, 8, 9, 10*
2	Positive Control (Fruit and vegetable compost waste + AlCl3)	1,67 ± 0,01	*4, 5, 9, 10*
3	White flour+AlCl3	1,64 ± 0,03	*4, 5, 9, 10*
4	Grechka (buckwheat) +AlCl3	1,11 ± 0,04	*All of them*
5	Cornmeal+AlCl3	1,27 ± 0,03	*All of them*
6	Rye Flour+AlCl3	1,83 ± 0,01	*1, 3, 4, 5, 9, 10*
7	Oat flour+AlCl3	1,79 ± 0,01	*1, 4, 5, 9, 10*
8	Barley flour+AlCl3	1,74 ± 0,03	*1, 4, 5, 9, 10*
9	Rice flour+AlCl3	2,85 ± 0,06	*All of them*
10	Wheat germ+AlCl3	4,19 ± 0,10	*All of them*

6. Conclusion and Discussion

The present study is the first report of a comparative analysis examining the effect of eight different cereal varieties on aluminum chloride-induced Alzheimer's disease in the E. fetidae worm model.The available data on the protection of the central nervous system by cereals are still insufficient (Szwajgier et al., 2012). In this context, the study once again emphasizes the importance of Alzheimer's disease and proper cereal consumption. High doses of aluminum chloride (usually 200 mg/kg soil and above) reduce the survival rate of worms.Zhang Jia'en et al. (2013) study showed that worms exposed to 200 and 300 mg/kg Al (aluminum) concentrations had 100% survival for the first 7 days, but this rate decreased with time. In our study, the survival rate of worms in the

buckwheat-fed diet group was observed to be 100% under conditions induced by 600 mg/kg AlCl3 over a ten-day period. This finding showed that despite the 600 mg/kg $AlCl_3$ concentration, the worms in the grechka-fed diet group exhibited high hardiness.

In the study, behavioral changes in learning and memory performance of animals after neurodegeneration due to AlCl3 were analyzed using the Seymour mechanism and duplo base plate, and limitation of movement due to aluminum chloride caused a paralysis-like formation to be observed in many experimental animals.In the diet groups containing wheat germ and rice flour, increased acetylcholinesterase activity led to a prolongation of the time spent on the Duplo baseplate. This finding suggests that overactivity of acetylcholinesterase may cause imbalances in synaptic transmission. In the study, it was observed that the responses of animals in various diet groups to light were significantly reduced. In particular, the higher locomotor skills in the diet groups containing grechka and cornmeal than in the positive control group may indicate the potential of some bioactive compounds in these nutrients to act as acetylcholinesterase inhibitors.AChE is the primary cholinesterase in animals, and decreased AChE activity signals a higher level of acetylcholine, a neurotransmitter substance.Statistical analyses performed in the study showed that different grain diets produced significant changes in AlCl3-induced AChE activity.Lower AChE activity was observed, especially in the Grechka and cornmeal groups, indicating that these cereals may be protective against the neurotoxic effects of AlCl3 in E. fetidae individuals. It has been found to be the most effective cereal type in AlCl3-induced Alzheimer's disease.The results of the analysis in the diet groups fed with wheat germ and rice flour, which showed high AChE activity, revealed that these grains did not have a protective effect against AlCl3.The differences in AChE activity observed in the study suggest that it may be due to dietary components altering the neurotoxic effect of AlCl3 in worms.

Referances

[1] Akman, Ö., Atasever, S., Güçlü, E., & Gümüş, G. (2011). Alüminyum ve İnsan.

[2] Albayrak, G., Demir, S., Koyu, H., & Baykan, S. (2022). Anticholinesterase compounds from endemic Prangos uechtritzii. Chemistry & Biodiversity, 19(11), e202200557.

[3] Breijyeh, Z., & Karaman, R. (2020). Comprehensive review on Alzheimer's disease: Causes and treatment. Molecules, 25(24), 5789.

[4] Canbolat, E., Yardımcı, H. (2016). Alzheimer hastalığı ve koruyucu besin öğeleri. Düzce Üniversitesi Sağlık Bilimleri Enstitüsü Dergisi, 6(2), 139-145.

[5] Campbell J.D.(1992) : Alüminyum ve Alzheimer hastalığı. Kasaba Lett Doktor Hasta, Temmuz. 1992.

[6] Hawkins K.E, Duchen M.(2019). "Modelling mitochondrial dysfunction in Alzheimer's disease using human induced pluripotent stem cells" World J Stem Cells. 11(5): 236–253.

[7] Kent, M. (2015). Advanced biology. Oxford University Press-Children.

[8] McKevith, B. (2004). Nutritional aspects of cereals. British Nutrition Foundation Nutrition Bulletin 29:111-142

[9] Nonaka S., Nakanishi H.(2019). "Microglial clearance of focal apoptotic synapses" Neurosci Lett. 5:134317
.

[10] Seymour, M. K. (1969). Locomotion and coelomic pressure in Lumbricus terrestris L. Journal of Experimental Biology, 51(1), 47-58.

[11] Subaraja, M. ve Vanisree, A.J(2019). Centella asiatica'dan izole edilen yeni fito bileşen asiaticoside-D, Lumbricus terrestris'in rotenon dejenere serebral ganglionlarında monoamin oksidaz-B engelleme potansiyeli sergiler. Phytomedicine , 58 , 152833.

[12] Szwajgier, D., & Borowiec, K. (2012). Phenolic acids from malt are efficient acetylcholinesterase and butyrylcholinesterase inhibitors. Journal of the Institute of Brewing, 118(1), 40-48.

[13] Şanlıer, N. (2012). Tam tahıl ürünleri ve sağlık üzerine etkileri. Tam Buğday Ekmeği Yaygınlaştırma Sempozyumu, ss, 48-54.

[14] Walton, W. R. (1927). Earthworms and light. Science, 66(1701), 132-132.

[15] Wilson, W. J., Ferrara, N. C., Blaker, A. L., & Giddings, C. E. (2014). Escape and avoidance learning in the earthworm Eisenia hortensis. PeerJ, 2, e250.

[16] Zhang Jia'en, Z. J. E., Yu JiaYu, Y. J., Ouyang Ying, O. Y., & Xu HuaQin, X. H. (2013). Responses of earthworm to aluminum toxicity in latosol.

AIR MUSCLE

Seyed Reza Hosseini , Iranian Cambridge School

ARTICLE INFO

Iran Team member, IYPT 2025, Lund University, Sweden

Advisors: Amirreza Soheili, Alireza Noroozshad

Accepted by Ariaian Young Innovative

Minds Institute , AYIMI

http://www.ayimi.org ,info@ayimi.org

ABSTRACT

Place a balloon inside a cylindrical net (as it sometimes used to wrap garlic) and inflate it. The net will expand and shorten. Investigate the properties of such a "muscle“. In this problem, we examine how a balloon inside a mesh structure behaves like a pneumatic artificial muscle, contracting under inflation. The phenomenon is analyzed using both experimental data and theoretical modeling.

Key Words : *Air Muscle, Balloon, Mesh, Inflation*

1. Introduction

A Pneumatic Artificial Muscle (PAM) is a pneumatic actuator for converting pneumatic power to pulling force. The PAM has advantages over conventional pneumatic cylinders such as high force to weight ratio, flexible structure, low cost and strong reliability for human use. According to the high force to weight ratio, the PAM can generate large pulling forces with the least amount of compressed-air consumption.

As in figure (1) there are different types of PAMs. The McKibben pneumatic artificial muscle, is one of the most famous artificial muscles and is most similar to our problem. Its structure is very simple The tube is covered with a mesh that can transform the growing air pressure inside the tube into a longitudinal force and displacement (Fig. 2).

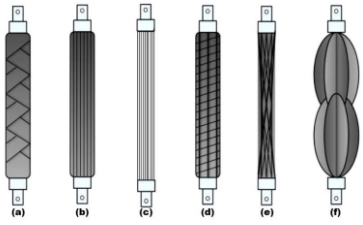

a) McKibben Muscle/Braided Muscle; (b) Pleated Muscle; (c) PAM reinforced by Kevlar Fiber; (d) Yarlott Netted Muscle; (e) Paynter Hyperboloid Muscle; (f) ROMAC Muscle.
(Kalita, B., Leonessa, A., & Dwivedy, S. K. (2022). *A review on the development of pneumatic artificial muscle actuators: Force model and application. Actuators, 11*(10), 288. https://doi.org/10.3390/act11100288)

Fig. 1: Different types of PAMs

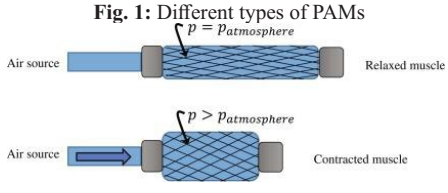

https://www.sciencedirect.com/topics/engineering/pneumatic-artificial-muscle

Fig. 2: Contraction in PAM

To find a clear relationship between the pressure inside the balloon and the force produced by the muscle and also. how much force this type of actuator can generate, and what factors affect that , some experiments are needed.

This may lead us to ask whether the force can be increased for example, by changing the material or geometry and finally, since the system relies on elastic materials,whether the muscle might weaken or lose performance over time. These questions became the foundation for both the theoretical and experimental parts of this research.

The theoretical model was developed to understand how the air muscle works. Then, the initial experimental setup is explained and how it evolved into a more refined version to improve accuracy and control.

2. Artificial Muscle Modeling

In this phenomenon, a balloon is placed inside a flexible but inextensible mesh. When air is pumped into the balloon, the internal pressure increases, causing the balloon to expand in diameter while contracting in length, exerting a pulling force is investigated (Fig. 3).

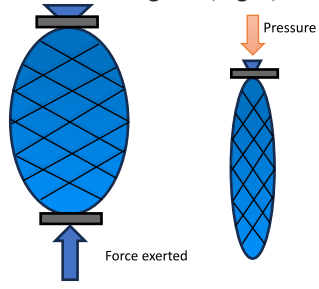

Fig. 3: Artificial Muscle modeling

Like real muscles, air muscles shorten in length while expanding outward, creating axial force. In air muscles, this behavior results from internal pressure acting against a constraining mesh.

3. Theoretical Model

To understand the contraction behavior more precisely, the geometry of the mesh structure was analyzed. The balloon is surrounded by a braided mesh which each of these elements are changed during inflation.To quantify the force generated by the muscle, the forces acting on a single element in the mesh is analyzed. The tension force T is the force along each fiber strand, pulling outward due to the internal pressure. The axial force F is the total force exerted along the muscle's length, this is the force responsible for performing mechanical work during

contraction. Using trigonometry, we relate these forces. This equation shows that the force depends nonlinearly on the radius, internal pressure, and fiber layout, capturing how the air muscle converts radial expansion into axial contraction force (Fig. 4).

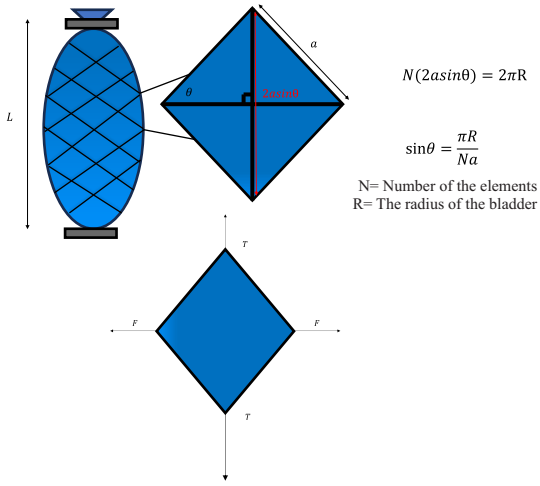

$$N(2a\sin\theta) = 2\pi R$$

$$\sin\theta = \frac{\pi R}{Na}$$

N= Number of the elements
R= The radius of the bladder

Fig. 4: Geometry model

$$\tan\theta = \frac{T}{F}$$

$$T = PDa\cos\theta$$

$$F = PDa\cos^2\theta/\sin\theta$$

Force Equation

$$F = \frac{2Pa\left(1 - \frac{\pi^2 R^2}{N^2 a^2}\right)}{\frac{\pi}{Na}}$$

- P – Pressure inside the bladder
- D – Diameter of the bladder
- a – the length of the side of a rhombus

Radius denoted simply as R in our force formula. However, that radius was actually the maximum radius of the balloon's cross-section what we now define more precisely as R_{max} .

This was a useful starting approximation, but it oversimplifies the geometry of the balloon. In reality, the radius varies along the horizontal axis of the balloon. It's largest at the center and decreases symmetrically towards the sides. To account for this, the model was refined by introducing a position-dependent radius, R(x), which represents the radius of the balloon at a specific horizontal distance x from the center. Since the cross-section is a circle, R(x) can be derived from the Pythagorean theorem and is given by:

$$R(x)=\sqrt{R_{max}^2 - x^2}$$

This formula captures the true shape of the balloon and will allow us to make more accurate calculations of the overall force, especially when integrating over its surface or length.

$$R_x = \int \sqrt{R_{max}^2 - x^2}\,dx$$

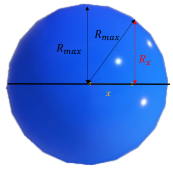

4. Experiment

To begin with, I used a rudimentary setup to observe the basic behavior of the muscle. This helped me understand how it contracts, how pressure affects its movement, and which variables might be important to control.

For inflation, a manual air pump was used by attaching a pressure gauge to monitor the internal pressure of the balloon in real time. To prevent any air leakage back into the pump, a ball valve was used between the pump and the balloon. This ensured that once the balloon was pressurized, the air would remain trapped. An air release system could easily reset the balloon between measurements. A spring dynamometer measured the force generated by the muscle . It was connected to one end of the mesh-covered balloon, so as the balloon expanded and contracted, the pulling force could be directly read from the scale. The setup was kept as simple and controlled as possible while still capturing the core behavior of the air muscle (Fig. 5).

Fig. 5: Initial Experimental Setup

5. Results

Accurate force values at each point, was obtained by Python to perform the numerical integration.

As predicted by our theoretical model, the force shows a cubic (third-degree) relationship with pressure (Fig. 6).

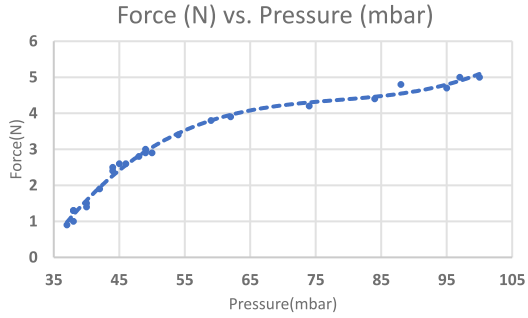

Fig. 6: Force vs. pressure

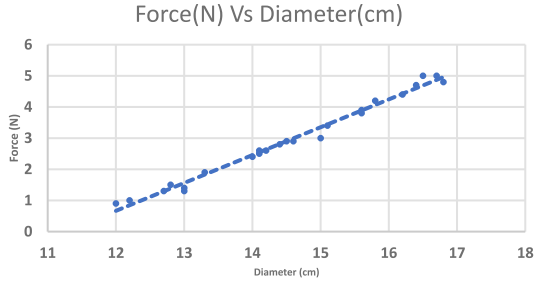

Fig. 7: Force vs. diameter

6. Experiment Extension

To obtain more accurate and consistent results, the experimental setup was refined . Instead of using a balloon, a latex tube was used to investigate key parameters such as **diameter, length, and pressure**

without the irregularities often seen with standard balloons inside a mesh. Additionally, the air muscle was now mounted vertically, which helped reduce friction and ensure more reliable force measurements (Fig. 8).

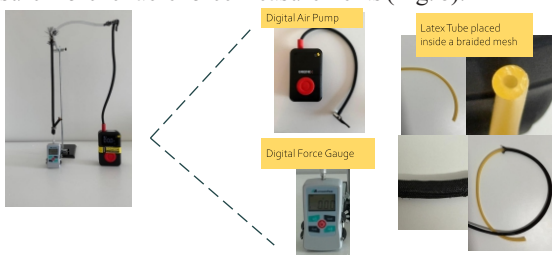

Fig. 8: Refined experimental setup

A range of lengths from 34 to 5 centimeters were tested to observe how contraction behavior changes with size. Also four different latex tubes were used with varying inner and outer diameters to study the effect of geometry. Tubes 3 and 4 were particularly useful for comparing the influence of wall thickness, since they had the same outer diameter but different inner diameters (Table 1).

Table 1: Parameters investigated

Parameter	Details
Lengths	34, 30, 25, 20, 15, 10, 5 cm
Latex Tube 1	Outer: 3/8", Inner: 1/4"
Latex Tube 2	Outer: 1/2", Inner: 5/16"
Latex Tube 3	Outer: 1/4", Inner: 1/8"
Latex Tube 4	Outer: 1/4", Inner: 3/16"
Wall Thickness Comparison	Tube 3 (thick) vs Tube 4 (thin)
Pressures	Multiple pressure levels tested

Next a latex tube was tested with an outer diameter of half an inch and five-sixteenths of an inch.The results were consistent (Fig. 9).

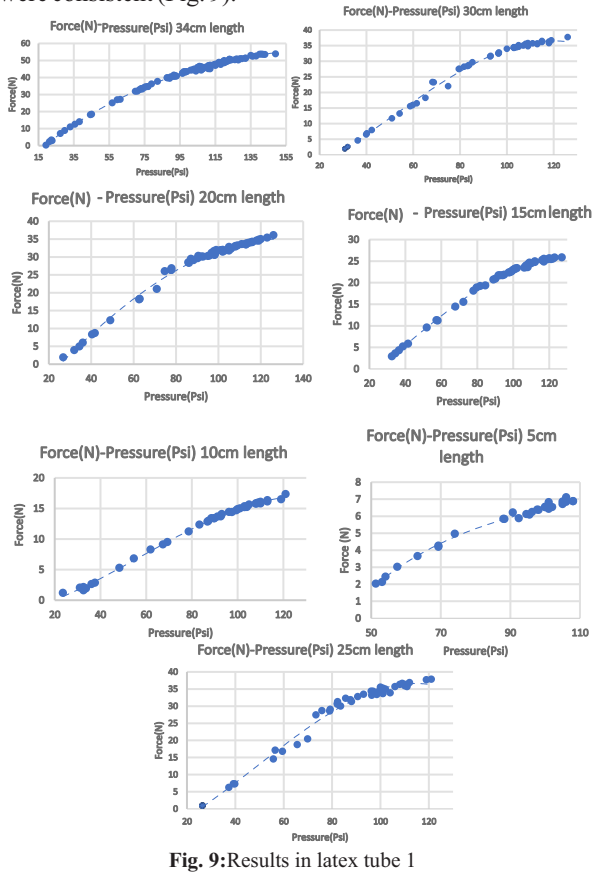

Fig. 9: Results in latex tube 1

These next four slides show the experiments I conducted with four different latex tubes. For each tube, I tested it at multiple lengths to collect data on its behavior under different conditions. The graphs shown on the display the results of one of the experiments I conducted using a latex tube with an outer diameter of 3/8 of an inch and an inner diameter of a ¼ of an inch, and measured how the force changes as the pressure increases.

You can see here that the relationship between force and length is cubic.

As the pressure increases, the force increases as predicted in the theoretical model. This trend was consistent across multiple trials (Figs. 10-12).

Latex tube 2: Diameter: 1/2 inch overall 5/16 inch inside

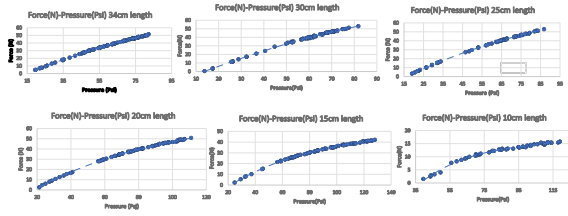

Fig. 10: Results in latex tube 2

Latex tube 3: Diameter: 1/4 inch overall 1/8 inch inside

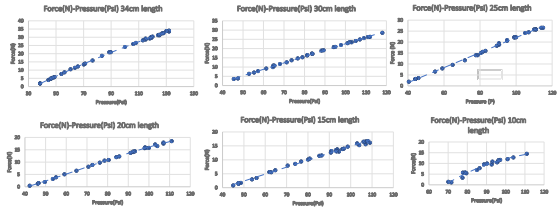

Fig. 11: Results in latex tube 3

Latex tube 4: Diameter: 1/4 inch overall 3/16 inch inside

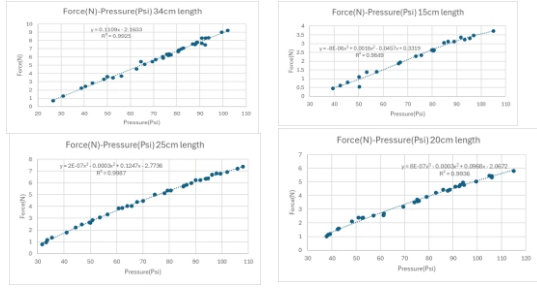

Fig. 12: Results in latex tube 4

To characterize the mechanical properties of each latex tube, a stress–strain experiment was conducted.

For each tube, increasing force was applied to measure the corresponding extension, then stress and strain. On these graphs, the x-axis shows strain (which is the relative change in length), and the y-axis shows stress (force divided by cross-sectional area).

In the elastic region, the relationship is linear and the slope of the linear fit gives the elastic modulus, which tells how stiff the material is.

Comparing the slopes across different tubes was used to quantify how material stiffness varies, and how that affects the air muscle's performance (Fig. 13).

Here, all the individual force–pressure graphs were placed for different muscle lengths side by side. Visually, we can see that as the initial length increases, the force measured at a given pressure also increases.

To investigate this further, force versus initial length was

model does not predict that force depends directly on length.

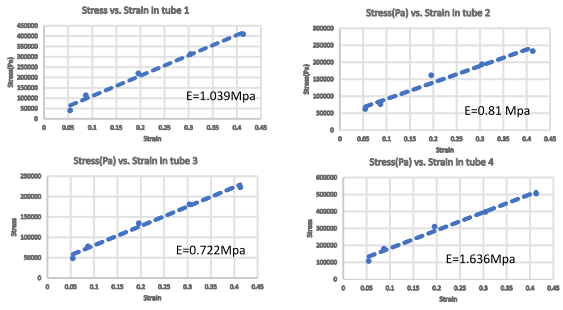

Fig. 13: Elastic module for each tube

However, as we discussed earlier, this behavior is due to how the force gauge operates. It measures displacement based restoring force, so longer muscles create larger displacements at the same pressure, resulting in higher force readings.

This shows the importance of understanding not only the physical system, but also how measurement tools influence the data.

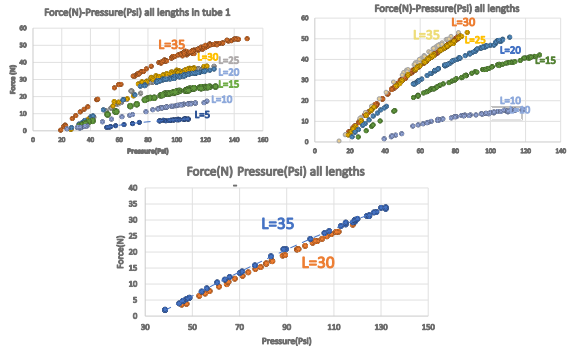

Fig. 14: Analysis on the impact of Length

This discrepancy is due to the force gauge being sensitive to displacement. Longer muscles contract over a greater distance, which leads to larger deflections in the gauge and artificially increases the measured force. This highlights a measurement artifact rather than a true increase in force output (Fig. 15).

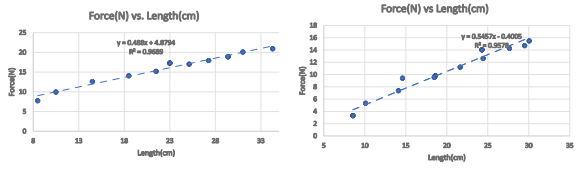

Fig. 15: Analysis on the impact of Length

The results showed that tubes with larger diameters produced greater force at the same pressure. This trend is consistent with the theoretical model presented earlier, which predicted a dependence of force on diameter.

The results further confirm that diameter plays a significant role in the performance of pneumatic artificial muscles (Fig. 16).

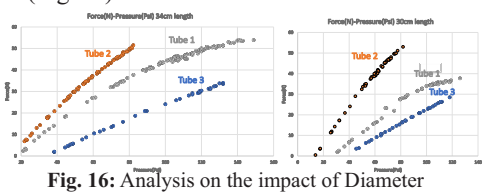

Fig. 16: Analysis on the impact of Diameter

Our initial assumption was that higher modulus materials produce more force. However, our experiments showed that a lower-modulus, thicker tube produced more force. This suggests that the increased radial expansion due to lower elasticity led to greater axial contraction and the thicker walls contributed additional restoring force. Both factors combine to increase the output force (Fig. 17).

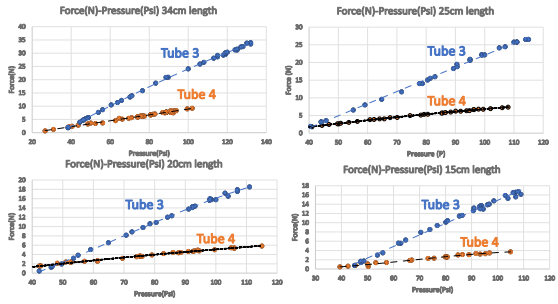

Fig. 17: Analysis on the impact of thickness

Next, the force produced during inflation and deflation was investigated . The hysteretic behavior observed during contraction and relaxation cycles is shown in figure (18). The loading and unloading curves do not overlap, indicating energy loss in the system. This behavior is primarily caused by friction. It's a key factor to consider when evaluating the efficiency and repeatability of the muscle.

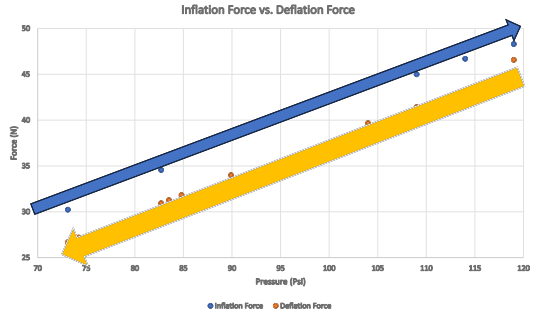

Fig. 18: Hysteretic Behavior

7. Results

Theory vs. experiment shows that our theoretical model matches really well with the experimental data. This strong agreement tells us that our assumptions are reasonable and that the model can reliably predict the behavior of the system. Any small differences are likely due to material imperfections or measurement errors. Overall, this gives us confidence in our approach (Fig. 19).

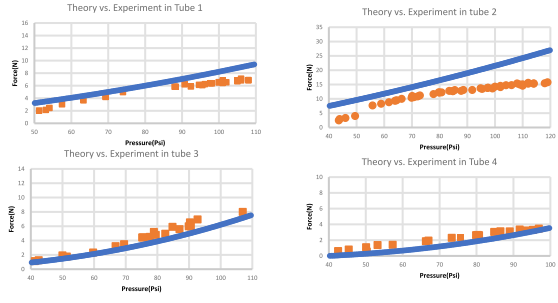

Fig. 19: Theory vs. Experiment

The theoretical surface to our experimental data in 3D is

compared. The theory shows that initial length does not affect the force . The reason is as explained before because how force gauge operates (Fig. 20).

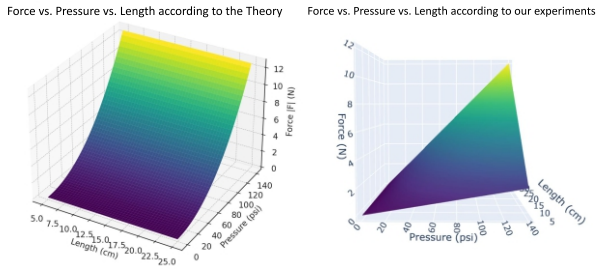

Fig. 20: Theory vs. Experiment in 3D

In the refined setup, a normal balloon inside a mesh was tested , similar to the original concept to find how different mesh types affected the produced force also different types of balloons to see how variations in size influenced the performance (Fig. 21).

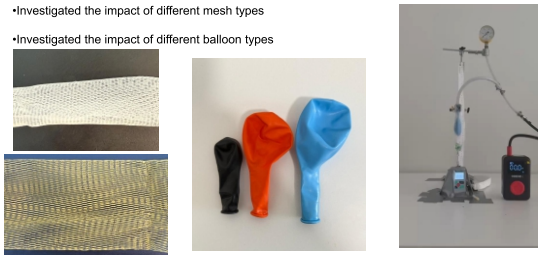

Fig. 21: Refined experiments with balloons

By comparing two meshes with different stiffness it is found the more flexible mesh had a pressure limit of around 70 mbar, after which it began to deform and lose effectiveness. In contrast, the stiffer mesh held its shape and continued generating force up to its pressure limit of about 110 mbar (Fig. 22).

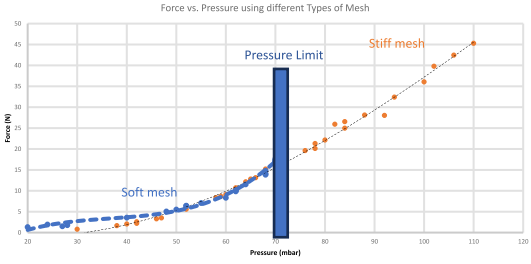

Fig. 22: Analysis on the impact of the mesh

How does the size of the balloon affect when it starts producing force? All the balloons eventually generate similar force once they're fully expanded and pressing against the mesh. But the smaller balloon takes more pressure to reach the mesh, so it starts producing force later than the larger ones (Fig. 23).

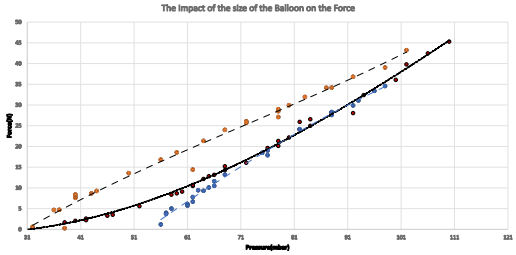

Fig. 23: Analysis on the impact of the size of the Balloon

To better understand how pneumatic artificial muscles compare to biological muscles, we used OpenSim to simulate a bicep contraction. Like our air muscle, the biological muscle shortens and generates pulling force, causing joint movement. This comparison helps us validate the usefulness of PAMs in replicating real muscle behavior (Fig. 24).

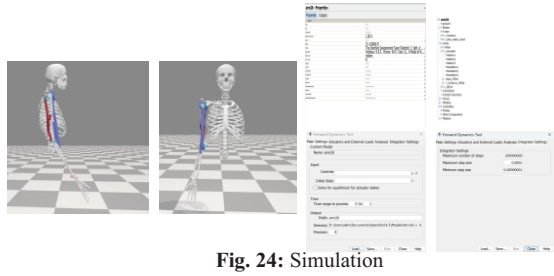

Fig. 24: Simulation

8. Real Life Applications

This is a simple demonstration I built to show a real-life application of pneumatic artificial muscles.

"Here, an air muscle contracts when compressed air is applied, causing the arm to lift a glass."

The motion closely mimics how a human biceps lift the forearm , it's smooth, quiet, and responsive. What's impressive is that this muscle is lightweight but generates enough force to lift a solid object with ease. This kind of setup is similar to what's used in assistive devices, soft robotics, or even exoskeletons (Fig. 25).

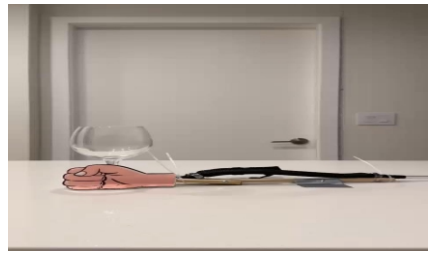

Fig. 25: Robotic arm

9. Conclusion

To summarize the theoretical model, we derived an expression for the force generated by the artificial muscle as a function of several key parameters: the internal pressure applied, the angle of the mesh, the diameter or radius of the inner bladder, and the number and geometry of the rhombuses formed by the mesh. These variables all influence how the muscle contracts and how much force it can output.

For the experimental setup we first used a rudimentary setup to observe how an air muscle generally behaves.

Then we refined the setup mounting the muscle vertically and using more precise equipment. We conducted multiple tests investigating different parameters such as the length, diameter, thickness, mesh type and bladder size.

According to the experiments it was observed that the force increased with pressure in a nonlinear way, which matches our theoretical predictions. Several physical factors impacted the output force including the mesh structure, the diameter of the tube, and the initial length of the muscle. We also found that both the thickness and the elasticity of the material played a role. Another key observation was hysteresis: the muscle did not follow the same path during contraction and relaxation, likely due to internal friction. Overall, the experimental results align well with the theoretical model we developed.

References

[1] Chou, C.-P., & Hannaford, B. (1996). Measurement and modeling of McKibben pneumatic artificial muscles. IEEE Transactions on Robotics and Automation, 12(1), 90–102. https://doi.org/10.1109/70.481753

[2] Jobbágy, B., Šimšík, D., Karchák, J., & Onofrejová, D. (2014). Robotic arm with artificial muscles in rehabilitation. Procedia Engineering, 96, 195–202. https://doi.org/10.1016/j.proeng.2014.12.143

[3] Kalita, B., Leonessa, A., & Dwivedy, S. K. (2022). A review on the development of pneumatic artificial muscle actuators: Force model and application. Actuators, 11(10), 288. https://doi.org/10.3390/act11100288

[4] Petre, I. M. (2021). Studies regarding the use of pneumatic muscles in precise positioning systems. Applied Sciences, 11(21), 9855. https://doi.org/10.3390/app11219855

[5] Tondu, B., & Lopez, P. (2000). Modeling and control of McKibben artificial muscle robot actuators. IEEE Control Systems Magazine, 20(2), 15–38. https://doi.org/10.1109/37.833638

[6] Wickramatunge, K. C., & Leephakpreeda, T. (2010). Study on mechanical behaviors of pneumatic artificial muscle. International Journal of Engineering Science, 48(2),188–198. https://doi.org/10.1016/j.ijengsci.2009.08.001

DANCING SLINKY

[a] Atoosa Esmaeili , [b] Mehraveh Zhegoulirani , a) Farzanegan 2 high school, b) Iranian Cambridge high school

ARTICLE INFO

a) Iran team member , IYPT 2025, Lund University Sweden

b) Iran team member, AYPT 2025, Montana University, Austria

Advisors: Mohammad Mahdi Shariatmadar,

Alireza Noroozshad

Accepted by Ariaian Young Innovative

Minds Institute , AYIMI

http://www.ayimi.org ,info@ayimi.org

ABSTRACT

Slinky, is a spring that oscillates under its own weight without any additional mass attached to it. By twisting a slinky several times and keep its bottom fixed, after releasing the top, the slinky starts to "dance" – wave-like phenomenon can be observed from the side-view. Suspended slinky may show different oscillation patterns and oscillation motion. These phenomenon and findings can be verified experimentally by considering its oscillations .

Keywords: *Slinky, Oscillation, Twisting, Dancing*

1. Introduction

A Slinky is a soft spring, made from plastic or steel. It was invented in the1940s and patented in 1947 by James. It has many interesting properties that show the interplay between kinetic energy, elastic potential energy, and gravitational potential energy. By releasing a slinky that is in a vertical orientation the bottom part of the slinky remains stationary until the top half descends to the point where the tension in the springs reduces such that the weight of the spring is more than the spring force.

Holmes et al. presented a model of a Slinky for calculating the equilibrium state of a Slinky for a range of end conditions. Their model included the effects of torsion, shear, and axial stress. More recently, Cumber demonstrated that for many scenarios the torsion spring representation reproduced the behaviour that Holmes et al. investigated. Shear and axial stress are important where the Slinky is on a slope and the slope is slowly increased or the Slinky is attached to two surfaces that are very close to each other relative to the unstretched length of the spring.

This system shows rich dynamics due to the interplay of elasticity, gravity, and oscillations There are the key parameters observed in this phenomenon as:

- Length (height)
- Number of Coils
- Diameter
- Angle of Twist
- Thickness of the coils
- Material

The dancing slinky problem involves a vertically slinky fixed at the bottom and twists from the top. When driven at certain frequencies, the slinky displays complex motion: some parts seem to float, some oscillate intensely and standing waves can also be observed (Fig.1).

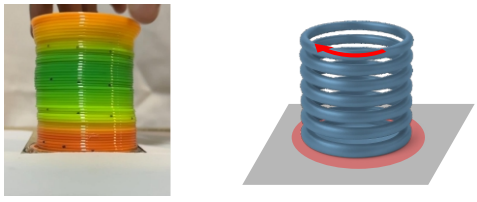

Fig. 1: The slinky

When the slinky is driven from the top, it stores energy as twisting (torsional) potential energy, which generates different types of waves torsional, longitudinal, and some transverse. The initial torque travels down as a torsional wave, and the slinky's elastic restoring force creates oscillatory motion. Damping also plays a role, gradually reducing the amplitude unless the motion is continuously driven (Fig. 2).

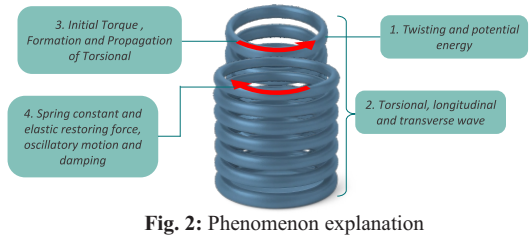

Fig. 2: Phenomenon explanation

2. Materials and Method

When we twist the slinky, the coils rotate around the central axis. This causes a change in the internal stress distribution. As a result:

The height of the slinky increases, because the coils stretch slightly apart.

The diameter decreases, because the coils pull inward.

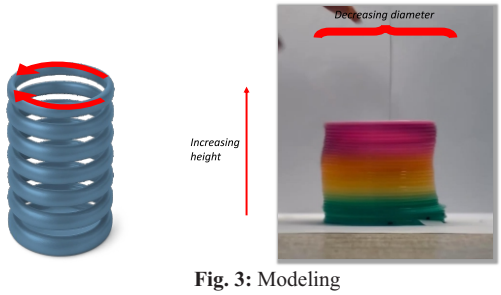

Fig. 3: Modeling

There is two types of springs, normal and torsional. A normal spring resists being stretched or compressed in a straight line. A torsional spring resists twisting instead of stretching.

To model the behavior of the slinky under twisting, we treat it as a torsional spring. The basic equation for a torsional spring is: In our case, we simplify it to: Then we

apply Newton's second law for rotation. This is the equation of motion for rotational dynamics in the slinky. The left side, $I\ddot{\theta}$, is the rotational inertia it resists angular acceleration. This is the equation of motion for a simple torsional oscillator (Fig. 4).

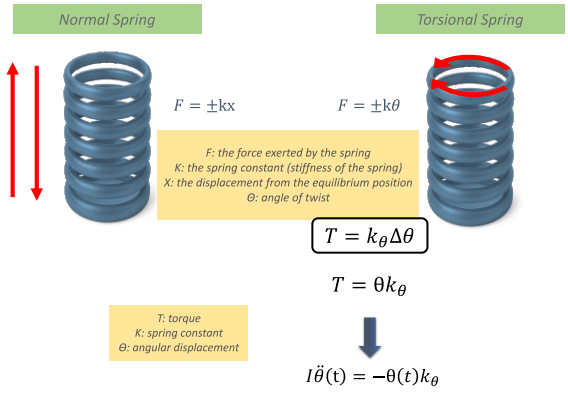

Fig. 4: Normal and torsional spring

3. Theoretical Model

Force Equations

$$I\ddot{\boldsymbol{\theta}}(\mathbf{t}) = -\boldsymbol{\theta}(\boldsymbol{t})\boldsymbol{k_\theta}$$

Rotational inertia ($I\ddot{\theta}$) → resists angular acceleration

$$I\ddot{\theta} = -k_\theta\theta - c_\theta\dot{\theta}$$

Damping ($c_\theta\dot{\theta}$) → resists motion, causes energy loss

$$T_{spring} = -k_\theta\theta$$

$$T_{damp} = -c_\theta\dot{\theta}$$

Restoring torque ($k_\theta\theta$) → tries to return the system to equilibrium

On the right side, we have two torques:
−k θ: the restoring torque, pulling the system back to equilibrium
−c θ ˙ : the damping torque, which resists motion and causes energy loss
Together, they describe the damped torsional oscillation of the slinky coils.

$$I\ddot{\theta}_N(t) + C\dot{\theta}_N(t) + k\theta_N(t) = 0$$

Moment of inertia — Angular Acceleration Effect — Damping Force Contribution — Elastic Restoring Force

The equation has been written is a second-order linear differential equation that describes the rotational motion of a damped torsional oscillator. Here in these terms the *I* demonstrate the moment of inertia. The second term represent the angular acceleration effect and the damping term is the equation for elastic restoring force.

After normalizing the equation of motion, the standard form of a damped harmonic oscillator is given which describes an oscillating system where:

• The amplitude decays exponentially over time due to damping. ω_d is the damped natural frequency, which is slightly lower than ω_n this means that when we twist the slinky, each segment oscillates back and forth while losing energy over time. The more damping we have, the faster the motion dies out. This model is essential to understand how torsional waves propagate and decay inside the slinky.

$$I\ddot{\theta}_N(t) + C\dot{\theta}_N(t) + k\theta_N(t) = 0 \Rightarrow \ddot{\theta} + 2\zeta\omega\ \dot{\theta} + \omega_n^2\theta = 0$$

Damping coefficient $\zeta = \frac{c_\theta}{2\sqrt{k_\theta I}}$ $\omega_n = \sqrt{\frac{k_\theta}{I}}$ Natural frequency without damp

$$\theta(t) = \theta_0 e^{-\zeta\omega_n t}\left(\cos(\omega_d t) + \frac{\zeta}{\sqrt{1-\zeta^2}}\sin(\omega_d t)\right)$$

$$\omega_d = \omega_n\sqrt{1-\zeta^2}$$ *system natural frequency*

Equations related to radial changes:

$$I\ddot{\theta}_N(t) + C\dot{\theta}_N(t) + k\theta_N(t) = 0$$

$$I = \frac{1}{2}mR^2$$

$$I(t) = \frac{1}{2}m\,R(t)^2$$

$$N(2R\pi) = L$$

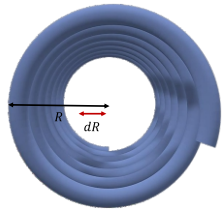

N: the number of coils
R: the effective radius
L: the total length of the Slinky extended

The equation signifies that the total length (L) experienced as a result of (N) twists in the slinky is equal to the number of twists multiplied by the circumference derived from its radius. This captures the relationship between the mechanical properties of the slinky when subjected to torsional stress.

$$(N + \Delta N)(2R'\pi) = L = N(2R\pi)$$

$$\frac{R'}{R} = \frac{N}{N + \Delta N}$$ ΔN: number of full twists

The elastic limit represents the maximum number that we can twist the slinky in this level when the slinky released it goes to fully returns to its original shape. But in plastic deformation level the slinky will deform completely (Fig. 5).

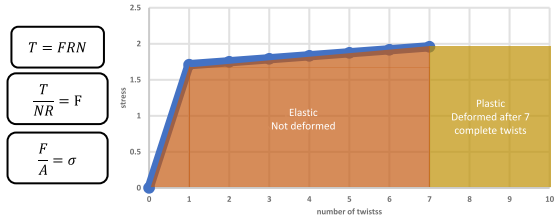

Fig. 5: Elastic and Plastic

4. Experiments

For experiment setup a rotating motor, a controller and different sizes of iron rods for different sizes of slinkies are used (Fig. 6) .

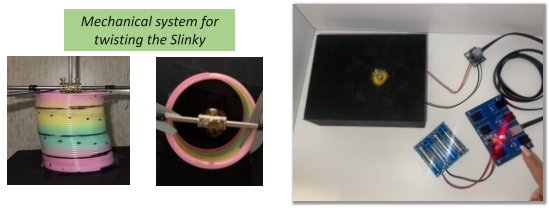

Fig. 6: Experimental setup

The horizontal rod is attached to the slinky and rotates with it, in a way that we could measure the angle of twist. A light was shining from above, and when the paper fell onto the mark we had made, it meant the slinky had rotated 360 degrees. For the fixed bottom, we used duct tape and completely fixed one coil onto the box. There was a 3 cm wooden base under the box, so it didn't move at all. For

recording two cameras were used one in front of the slinky and a camera on top .

5. Parameters Analysis

According to the experiments parameters such as angle of twists, diameter of the slinky, material of the slinky and number of coils are studied and theory vs experiments are compared.

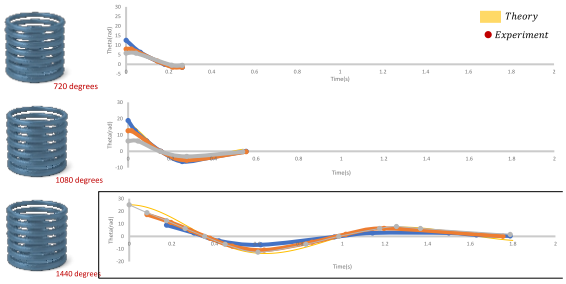

Fig. 7: Angle of twist

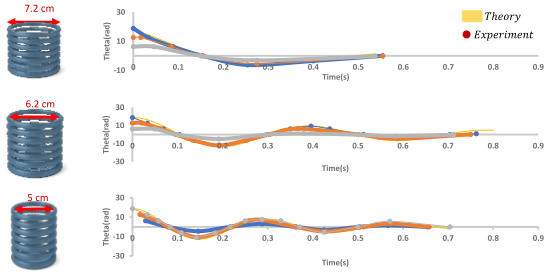

Fig. 8: Diameter of the slinky

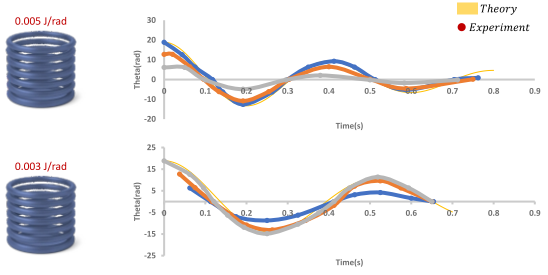

Fig. 9: Material of the slinky

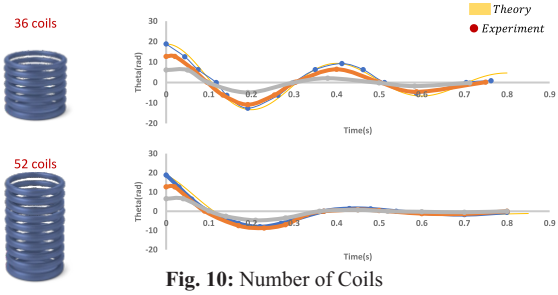

Fig. 10: Number of Coils

6. Conclusion

We modeled the slinky as a damped torsional oscillator with distributed mass and elasticity.

Each segment follows the rotational equation. By normalizing, we get the standard form of a damped harmonic oscillator, where the solution shows oscillatory motion with exponential decay.

Based on the fit between theory and experiment, it can be concluded that in the first setup, the equations used exhibit high numerical accuracy, and the tests performed involve a well-designed setup with minimal error.

Increasing the angle of twist stores more torsional potential energy in the slinky. This leads to stronger torsional waves and larger oscillation amplitudes.

A larger diameter increases the moment of inertia, which makes the slinky more resistant to angular acceleration. As a result, the natural frequency decreases, and the system responds more slowly to the same torque. The material determines the stiffness (torsional constant). A stiffer material leads to higher natural frequency and faster wave propagation. Increasing the number of coils increases the total mass of the slinky. It lowers the overall torsional stiffness, making the slinky oscillate at lower frequencies.

References

[1] P. Mohazzabi and B.M. Shefchik. A universal relationship between spring constant and torsion constant. J. Phys. Chem. Solids 62, 4, 677-681 (2001) .

[2] https://www.physics.colostate.edu/physics-demos/slinkies-and-springs

[3] Jörg Pretz. Oscillations of a suspended slinky. Eur. J. Phys. 42 (2021) 045008 (11pp). https://doi.org/10.1088/1361-6404/abcddf

[4] Peter S Cumber. International Journal of Mechanical Engineering Education, 2024, Vol. 52(3) 372–400Lagrange's method applied to a Slinky

Ariaian Young Innovative Minds Institute, AYIMI
Unit 14, No. 32, Malek Ave., Shariati St.
Post Code: 1565843537
Tel - Fax: +9821-77522395, 77507013
Tehran/ Iran
URL: http://www.ayimi.org
http://journal.ayimi.org
Email: info@ayimi.org